FRONTIERS OF PHYSICS

TOPICAL REVIEW
Volume 19 / Issue 1 / 13500 / 2024

Recent advances in memristors based on two-dimensional ferroelectric materials

Wenbiao Niu[1,#], Guanglong Ding[1,#], Ziqi Jia[1], Xin-Qi Ma[1], JiYu Zhao[1], Kui Zhou[1], Su-Ting Han[2], Chi-Ching Kuo[3,†], Ye Zhou[1,‡]

1 Institute for Advanced Study, Shenzhen University, Shenzhen 518060, China
2 College of Electronics and Information Engineering, Shenzhen University, Shenzhen 518060, China
3 Institute of Organic and Polymeric Materials, Research and Development Center of Smart Textile Technology, Taipei University of Technology, Taipei 10608, Taiwan, China
#These two authors contributed equally to this work.
Corresponding authors. E-mail: †kuocc@mail.ntut.edu.tw, ‡yezhou@szu.edu.cn
Received May 22, 2023; accepted July 3, 2023

© Higher Education Press 2023

ABSTRACT

In this big data era, the explosive growth of information puts ultra-high demands on the data storage/computing, such as high computing power, low energy consumption, and excellent stability. However, facing this challenge, the traditional von Neumann architecture-based computing system is out of its depth owing to the separated memory and data processing unit architecture. One of the most effective ways to solve this challenge is building brain inspired computing system with in-memory computing and parallel processing ability based on neuromorphic devices. Therefore, there is a research trend toward the memristors, that can be applied to build neuromorphic computing systems due to their large switching ratio, high storage density, low power consumption, and high stability. Two-dimensional (2D) ferroelectric materials, as novel types of functional materials, show great potential in the preparations of memristors because of the atomic scale thickness, high carrier mobility, mechanical flexibility, and thermal stability. 2D ferroelectric materials can realize resistive switching (RS) because of the presence of natural dipoles whose direction can be flipped with the change of the applied electric field thus producing different polarizations, therefore, making them powerful candidates for future data storage and computing. In this review article, we introduce the physical mechanisms, characterizations, and synthetic methods of 2D ferroelectric materials, and then summarize the applications of 2D ferroelectric materials in memristors for memory and synaptic devices. At last, we deliberate the advantages and future challenges of 2D ferroelectric materials in the application of memristors devices.

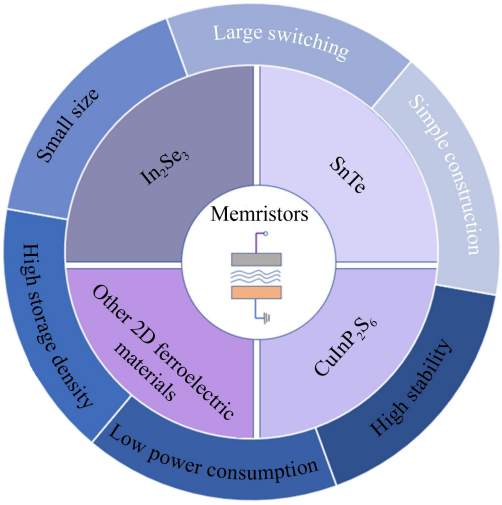

Keywords two-dimensional ferroelectric materials, synthesis strategies, memristors, artificial synapses

*Special Topic: Materials, Mechanisms and Applications of Memristors (Eds.: Xiaobing Yan, Bin Gao & Qi Liu).

Higher Education Press

https://doi.org/10.1007/s11467-023-1329-8

Contents

1 Introduction

With the coming of big data era and the improvement of information technologies, the demand for the data storage and processing devices with small size, high efficiency, and low energy consumption is increasing. However, the traditional computing system with von Neumann architecture is facing the challenges of memory walls resulted from the separated memory and data processing units (i.e., von Neumann bottleneck), and cannot meet this demand [1–3]. Human brain is a super computer with small size (1.5 L) and low energy consumption (20 W), which can realize in-memory computing and data parallel processing, and the high performance of brain is on the basis of its highly developed neural network consisting of large numbers of neurons (10^{11}) and synapses (10^{15}) [4–6]. Therefore, by mimicking the structure of brain, developing high performance neuromorphic devices that can imitate the behaviors of synapses/neurons, and further building artificial neural networks (ANNs) is one of the most efficient ways to break von Neumann bottleneck and realize the data storage/processing with low power consumption and high efficiency [7–10].

The most common neuromorphic devices can be broadly divided into two types: memristor and transistor. Memristor is one kind of two-terminal device with metal–insulator–metal sandwich structure, which was demonstrated experimentally by Hewlett–Packard Labs in 2008 [11–13]. In 1971, Chua [14] proposed the existence of a fourth component in addition to resistive, capacitive, and inductive circuit elements – the memristor. Compared to transistor type neuromorphic devices, memristor has the advantages of simple structure, good stability, low power consumption, and high integration density [15–17]. Memristor represents the relationship between charge and magnetic flux, and the magnitude of its resistance value will change with the amount of current flowing through it, presenting a nonlinear resistance characteristic with memory function [18–20]. By applying electric field to one electrode and grounding the other one, the insulator changes to a high resistance state (HRS) or low resistance state (LRS) depending on the voltage polarity, the construction of the device, and the material properties. When the resistive state of the insulating material changes from HRS to LRS, it is considered as a "write" process, and conversely, "erase" process [21]. Currently, there are various kinds of materials for developing memristors, including metal oxides [22–26], 2D materials [27–30], biomaterial [31, 32], perovskite [33–36], polymers [37–39], etc.

Due to the excellent electrical properties, the application of 2D materials in memristor has attracted lots of attention [40, 41]. Ferroelectric materials represent a class of materials with ferroelectric effects, whose dipoles can be polarized spontaneously within a certain temperature range, and the polarization direction can be changed by the applied electric field [42]. Due to the adjustability of polarization under external factors, ferroelectric materials are usually multifunctional with piezoelectricity, dielectricity, pyroelectricity, and optoelectronic characteristic in addition to ferroelectricity [43–46]. Benefitting from the multifunctional features, ferroelectric materials have been applied in various important fields, including nonvolatile data storage devices [47, 48], ferroelectric field effect transistor [49, 50], piezoelectric flexible sensors [51, 52], pyroelectric sensors [53, 54], solar cells [55] and photodetectors [56], and established as one of the research hotspots and frontiers in some advanced technology fields in recent years, such as network communications, home appliances, medical electronics, and national defense [57–60]. The ferroelectricity in 2D materials (SnTe) has been discovered for the first time by Chang *et al.* [61] in 2016, which brought important functions and opportunities to the 2D material family. In recent years, 2D ferroelectric materials have been widely applied in memristors due to the exceptional advantages of ferroelectricity, which not only improve the device performance, but also promote the applications in low-power consumption devices, flexible electronics, high-temperature systems, and neuromorphic computing [40, 62].

Studies for achieving brain-like synapses functions with memristor based on 2D ferroelectric materials are conducted in the past few years and rapidly developed. Therefore, it is necessary to summarize the recent devel-

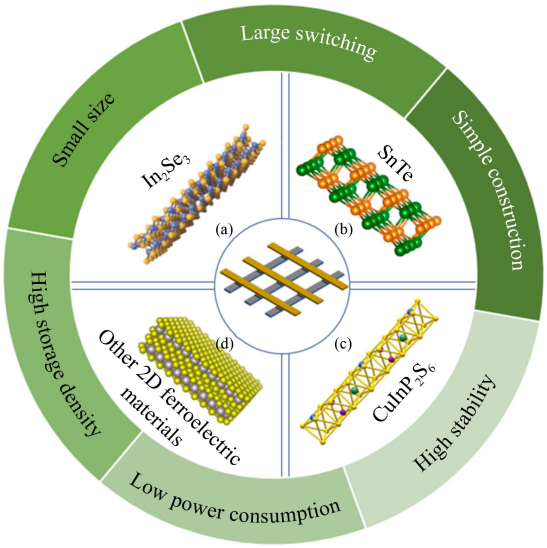

Fig. 1 High performance of memristors based on several kinds of 2D ferroelectric materials. (a) Reprinted with permission from Ref. [63], Copyright © 2020 Wiley -VCH GmbH. (b) Reprinted with permission from Ref. [64], Copyright © 2019 American Chemical Society. (c) Reprinted with permission from Ref. [60], Copyright © 2021 American Chemical Society. (d) Reprinted with permission from Ref. [65], Copyright © 2022 American Chemical Society.

opment on 2D ferroelectric materials based memristors, providing references and directions for the future work. In this review, we focus on several kinds of 2D ferroelectric materials (Fig. 1), including In_2Se_3, SnTe, $CuInP_2S_6$, and other 2D ferroelectric materials. We first introduce the basic concepts and characters of 2D ferroelectric materials and memristors, then present the synthesis approaches of 2D ferroelectric materials briefly and discuss the applications of 2D ferroelectric materials based memristors in data storage and artificial synapses. Finally, we present the advantages and future challenges of 2D ferroelectric materials in the application of memristors devices.

2 Physical mechanism of 2D ferroelectric materials

The word "ferroelectric" is derived from "ferromagnetic" due to the similar hysteresis curve of ferroelectric materials under the electric fields with those of ferromagnetic materials under magnetic fields [66]. In Fig. 2(a), OD, OE, and OF represent the remanent polarization, spontaneous polarization, and the coercive electric field E_c, respectively. With the increase of electric fields, the polarization intensity of the ferroelectric body does not follow the electric field in a linear relationship, but shows a hysteresis relationship, which is the electric hysteresis curve.

In 1920, Valasek discovered the specific dielectric properties of Rochelle salt (potassium sodium tartrate), and measured its dielectric response, piezoelectric properties, pyroelectric phenomena, and other macroscopic properties, thus starting the history of ferroelectric materials [67]. In 1946, the ceramics ferroelectric $BaTiO_3$ was first prepared. It has great ferroelectric polarization properties, relatively high phase transition temperature, relatively large piezoelectric coefficient and dielectric constant [68, 69]. In the mid-80s, the high-quality ferroelectric thin films were successfully prepared benefitting from the important breakthroughs in the thin films' preparation technology, promoting the rapid development of electronic devices [70, 71]. The epitaxial growth of conventional three-dimensional (3D) ferroelectric films needs suitable lattice-mismatched substrates, which limits the application to a great extent. The conventional 3D ferroelectric materials are limited by the critical size effect, and their ferroelectricity is suppressed as the thickness becomes thinner, while they also tend to be "hard" and "brittle" due to the characteristics of the bulk phase, strong covalent or ionic bonding interactions, and the lack of interlayer slip mechanisms, which is not conducive to the application in flexible and thin devices [72, 73]. 2D ferroelectric materials with different structural properties can be stacked and used for ferroelectric heterostructure devices without the limitation of substrates, thus providing tunable ferroelectric properties [41, 74]. On the other hand, as the materials researches move into the realm of nanoscale and monolayer, more and more materials exhibit ferroelectricity. Therefore, due to the unique advantages of extremely thin thickness, excellent interfacial tunability, and low nanoscale applications, 2D ferroelectric materials have become one of today's research hotspots [75]. In recent years, various 2D ferroelectric materials, such as In_2Se_3 [63, 76, 77], $CuInP_2S_6$ [78–80], $MoTe_2$ [56, 81, 82], and MoS_2 [65, 83–86], have been applied in diverse applications such as electronic synapses, nonvolatile memory devices, photocatalyst, and ultraviolet photodetector.

The fundamental reason for ferroelectric polarization is due to the dipoles that are natural presence in ferroelectric materials [87]. For example, $CuInP_2S_6$ and α-In_2Se_3 are both 2D ferroelectric materials with room-temperature polarization characteristics, and belong to the displacement-type ferroelectric materials whose polarization arises from the displacement of Cu, In and Se atoms away from the center of symmetry, which is the same physical principle as the displacement of Ti atoms in the conventional ferroelectric material $BaTiO_3$ [88, 89]. In particular, Cui *et al.* [90] found that In_2Se_3 is characterized by in-plane (IP) and out-of-plane (OOP) polarizations at room temperature. To investigate the spontaneous ferroelectric polarization, the α and β phases of In_2Se_3 were studied using piezoelectric response force microscopy (PFM). The amplitude of PFM can show the magnitude of the local piezoelectric response, and the phase indicates the direction of ferroelectric polariza-

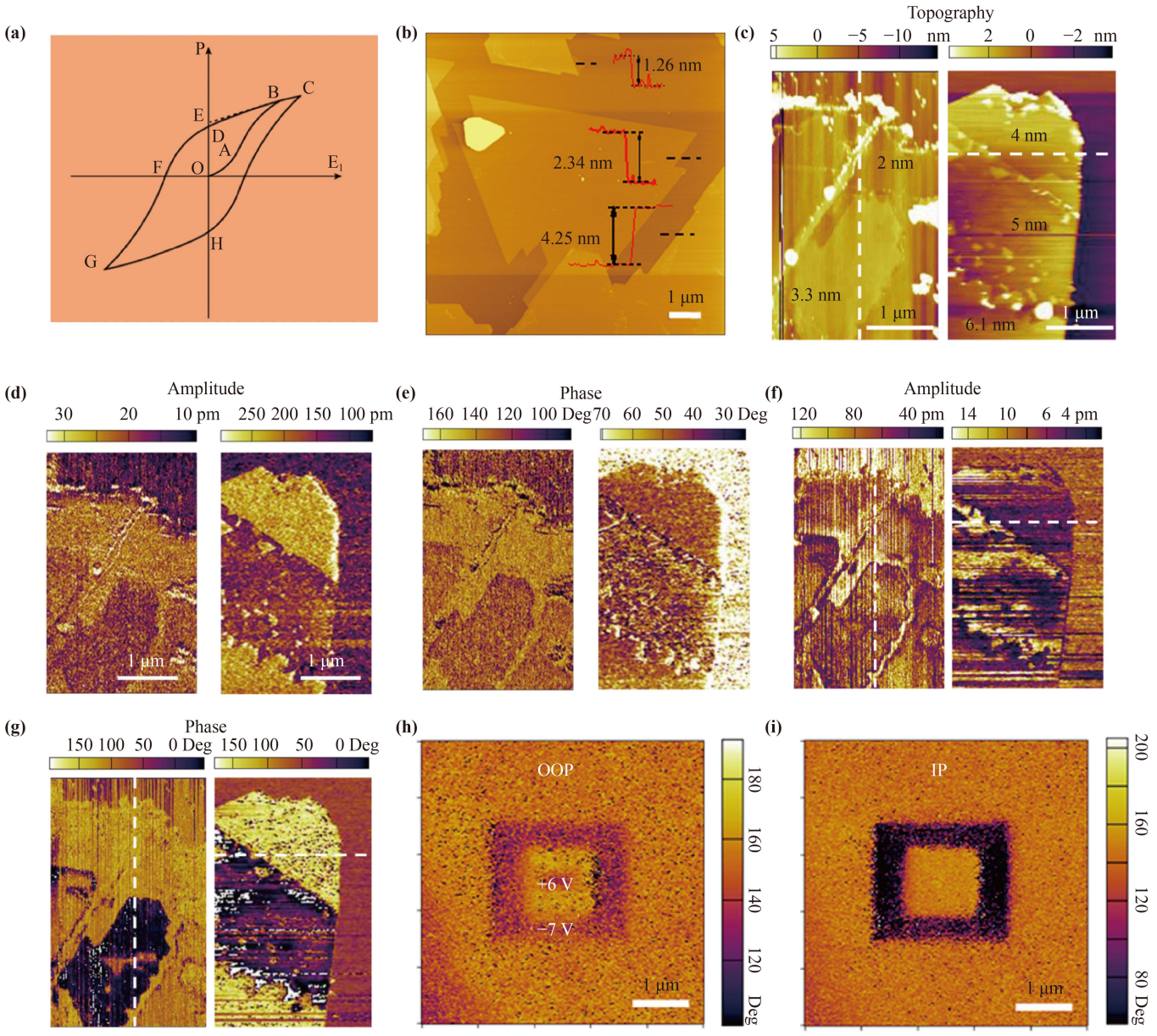

Fig. 2 **(a)** Hysteresis curve of ferroelectric materials under electric field. E1 represents the electric field. **(b)** AFM image of In_2Se_3 films with thicknesses of 1.26–4.25 nm. **(c)** AFM images of In_2Se_3 films at 2–6 nm. **(d, e)** Amplitude and phase images of OOP PFM. **(f, g)** Amplitude and phase images of IP PFM. **(h, i)** OPP and IP phase images corresponding to 6 nm In_2Se_3 flake obtained by applying successive voltages of –7 and +6 V with size of 2 and 1 μm. The scale bars are 1 μm in (b–i). (b–i) Reprinted with permission from Ref. [90], Copyright © 2018 American Chemical Society.

tion. It was found that different thicknesses of In_2Se_3 have different shape rules: when the thickness is ≥ 2 nm, it has a regular shape with good crystallinity; when the thicknesses is < 1.3 nm, it usually has an irregular shape, as shown in Fig. 2(b). Figure 2(c) shows the morphology of selected α-In_2Se_3 flakes with thicknesses of 2–6 nm. The OOP PFM amplitude and phase images of these flakes are shown in Figs. 2(d) and (e), and the corresponding IP PFM amplitude and phase images are shown in Figs. 2(f) and (g). We can observe that In_2Se_3 forms a single ferroelectric domain within each terrace, and IP polarization is greater than OOP polarization. PFM technique can also be used to characterize the polarization change under electric field. After transferring α-In_2Se_3 flakes onto a metal-coated Si substrate and then applying opposite voltages (–7 V and +6 V) with square patterns, the polarization changes in OOP and IP can be obtained by testing the phase variation, as shown in Figs. 2(h) and (i). In some 2D ferroelectric materials such as h-BN and MoS_2, their monolayers have the symmetric structure and do not yield ferroelectricity, but in their bilayers or multilayers, some stacking modes can disrupt their

spatially symmetric structure, producing OOP ferroelectricity, which can be achieved by interlayers slippage and flipping. It is a new ferroelectric mechanism and named sliding ferroelectricity [91–93].

Normally, the dipoles in a ferroelectric body would not spontaneously polarize in the same direction, but in a small region the dipoles have spontaneous polarization in the same direction approximately, and this small region is known as the ferroelectric domain walls [94]. The thickness of the domain walls is the result of various energy balances, and domain walls are different in direction due to their spontaneous polarization [23, 95]. At temperature higher than Curie temperature, the built-in electric field in ferroelectric materials disappears and there is no longer the nature of spontaneous polarization. The polarization of ferroelectricity is related to the external electric field, pressure, film thickness, polar axis properties, and the external temperature [96]. The above physical properties have led to growing interests in 2D ferroelectric materials and promoted the applications in various fields [51, 97, 98].

2.1 Piezoelectric effect

As the positive and negative charge centers of ferroelectric body do not coincide, they spontaneously produce electric dipole moments. When the ferroelectric body is deformed by an external force in a certain direction, its interior will be polarized, and positive and negative charges occur on two opposite surfaces. After removing the external force, it returns to its uncharged state, which is known as the positive piezoelectric effect [51, 99]. Conversely, when an electric field is applied along the direction of polarization of the ferroelectric body, it will also be deformed. After removing the electric field, the deformation disappears, which is named the negative piezoelectric effect [100].

2.2 Pyroelectric effect

The pyroelectric effect in ferroelectric materials refers to the charge release phenomenon resulted from the change of polarization intensity under different temperature [53]. Macroscopically, for ferroelectric materials, the change of temperature can produce the voltage or current at both ends of the materials. Due to the wide response range, high sensitivity, and easily adjustable performance, the ferroelectric materials with pyroelectric effect, can be used in energy conversion, detection devices, etc. [101].

2.3 Optical effect

Under the illumination condition, the excited electrons in the valence band or impurity energy levels in ferroelectric materials can jump to the conduction band. Therefore, ferroelectric materials can generate a steady-state current in short-circuited circuit [102]. Because of the strong light-matter interaction, ultra-thin structure, and current compatibility with silicon electronics, ferroelectric materials have attracted great interest in optoelectronic integration [103]. It is also possible to use lasers to optically modify 2D materials, including defect control [104], doping [105], and phase change [106].

3 2D ferroelectric materials and synthesis strategies

Since the successful isolation of graphene in 2004, many scientific researchers have conducted extensive studies and made various breakthroughs in 2D layered materials owing to their unique electrical, optical, mechanical, thermal properties, and potential applications in electronic components [107, 108]. In particular, 2D layered materials with asymmetric structures have gained more and more attention due to their promising electronic device applications, among which the ferroelectric materials have been increasingly favored in recent years owing to their relevant polarization and potential applications. The ferroelectrics with intrinsic van der Waals (vdWs) that have been discovered so far are basically 2D ferroelectric materials [109, 110]. Unlike conventional ferroelectrics with rigid crystals, 2D vdWs ferroelectrics exhibit stable layer structures under strong intra-layer forces and weak inter-layer forces. The combination of these special atomic arrangements and ferroelectric order gives rise to entirely new physical phenomena and functions, including piezoelectric effect, pyroelectric effect, and optical effect [111, 112]. Several representative 2D vdWs ferroelectric materials are In_2Se_3, $CuInP_2S_6$, SnTe, MXenes, MoS_2, $MoTe_2$, and so on.

3.1 α-In_2Se_3

In In_2Se_3, each monolayer consists of alternating layers of Se or In atoms connected by covalent bond. According to the stacking orders of layers, In_2Se_3 has a variety of crystalline phases (α, β, γ, δ, κ), which induces various physical properties [76]. The α-phase is found to be the most stable one at room temperature, whose lamellar structure and ferroelectric polarization can be maintained even when the thickness reaches its limit (monolayer) due to the intrinsic interlocking structure of the dipoles. In the structure of the lamellar phase, the basic structural framework consists of a sequence of atoms with strong covalent bonds, "Se–In–Se–In–Se", which is called quintuple layers (QLs). QLs are repeatedly stacked by vdWs forces. Due to the broken central symmetry of α-In_2Se_3, the ground state structure of the QLs has both spontaneous IP and OOP polarization [113]. Figure 3(a) shows a side view of the crystal structure of α-In_2Se_3. Figure 3(b)

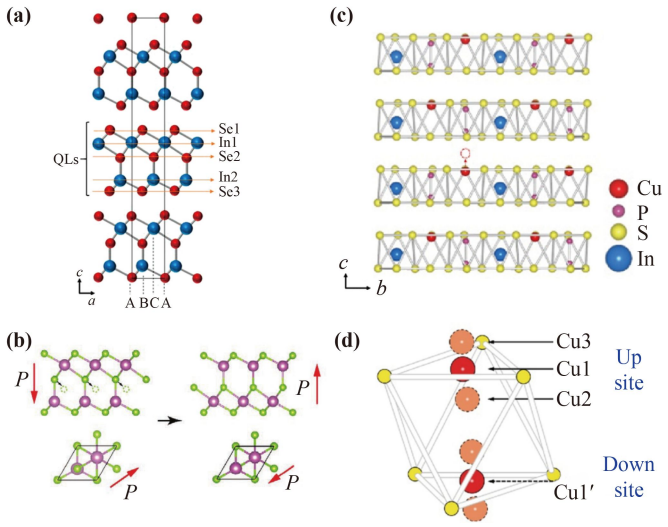

Fig. 3 **(a)** Side view of the crystal structure of α-In_2Se_3. **(b)** Schematic representation of the planar crystal structure and ferroelectric polarization $P\uparrow$ and $P\downarrow$ of α-In_2Se_3. **(c)** The sulfur framework of the $CuInP_2S_6$ crystal structure with octahedral gaps filled by Cu and In cations and P–P pairs, where Cu^+ ions can leap within the layer and cross the vdWs gap under the electric field. **(d)** The labelled Cu1, Cu2 and Cu3 are the three copper positions. The downward and upward positions of Cu1 are also denoted. (a) Reprinted with permission from Ref. [76], Copyright © 2021 American Chemical Society. (b) Reprinted with permission from Ref. [113], Copyright © 2020 Wiley-VCH GmbH. (c, d) Reprinted with permission from Ref. [79], Copyright © 2021 American Chemical Society.

shows the ferroelectric polarization properties of α-In_2Se_3. By using the excellent optoelectronic property some researchers have developed the optoelectronic synapses based on In_2Se_3, showing controllable temporal dynamics under electrical/optical stimulations [114]. In addition, an $In_2Se_3/CoIn_2/CoSe_2$ hollow nanorod structure can also be constructed and applied as electrode materials [115]. In_2Se_3 has excellent ferroelectric, optoelectronic, and thermoelectric properties that make it a great prospect for nonvolatile memory devices, strain sensors, optoelectronic devices, etc. [116].

3.2 SnTe

SnTe is an environmentally friendly 2D material due to its low toxicity. With the growing global demand to reduce the dependence on carbon-based fuels and energy waste, pyroelectric phenomenon is becoming one of the most attractive research topics in the sustainable energy field. SnTe has excellent pyroelectric properties, and has achieved significant progresses in the practical applications [117, 118]. Moreover, SnTe is a p-type candidate with high carrier concentration and intrinsic cationic vacancies. Recently, the doping effects on energy band and thermoelectric property of SnTe have been studied widely [119]. It has been shown that the doping of halogen atoms (Cl, Br, I) can adjust the Fermi level position to develop n-type SnTe, and plays a significant role in optimizing the thermoelectric property of the n-type SnTe [120]. For example, Pang *et al.* [121] found that the addition of Pb and I can inhibit the cation vacancies in SnTe, which allows to synthesize the n-type SnTe successfully, whose thermoelectric performance was also excellent.

3.3 $CuInP_2S_6$

$CuInP_2S_6$ (CIPS) is a 2D ferroelectric material and comprises a sulfur framework with octahedral voids filled by Cu, In and P–P triangular patterns. Cu^+ ions can leap within layers and cross the vdWs gap under the electric field as shown in Figs. 3(c) and (d) [79]. When the temperature is below the Curie temperature, the spontaneous polarization comes from the deviation of the Cu and In atoms from the center. The migration of Cu^+ ions in 2D CIPS can affect the electrical conductivity and result in the tunable rectification effect under the electric fields and other factors, which can be applied for developing synaptic devices to simulate various biological synaptic behaviors [122], and smart memristors [123], respectively. These studies have facilitated the development of synaptic devices and made CIPS an ideal material for memristors and ANNs. The heterojunction materials constructed by CIPS have also been applied to photocatalytic hydrogen production, presenting a new concept for the design and construction of ferroelectric materials for photocatalysis [80].

3.4 Other 2D ferroelectric materials

Recently, a kind of MXene material Nb_2NF_2 is demonstrated that it has good reversible OOP and metallic properties based on first-principles calculations, opening the door of exploring the properties of MXenes materials [124]. After that, a study proved that 2D $Ti_3C_2T_x$ MXene film has obvious ferroelectric hysteresis loops at room temperature and exhibits room-temperature ferroelectricity, and this research finding expands the application and development of 2D ferroelectric material [125]. Tahir *et al.* [126] investigated the relationship between the polarization of $Ti_3C_2T_x$ film and electric field at different frequencies, and the results showed typical ferroelectric behaviors at all frequencies, which proves the existence of its room temperature ferroelectricity. The memory device based on MXene shows bipolar switching with good stability and reproducibility, which opens a new path for 2D ferroelectric memory devices [126]. The ferroelectric materials with excellent electrical properties are not limited to the above. Transition metal dichalcogenides (TMDs) such as $MoTe_2$ and MoS_2 have

received great attention due to their excellent properties and unique structures. The single-atom characteristics of TMDs is a forceful strategy for the design of memristor with excellent applications. For example, Yuan *et al.* [127] reported the discovery of robust OOP ferroelectricity at room temperature in monolayer $MoTe_2$, and revealed the physical mechanisms behind it by theoretical calculations and structural characterizations. In their study, vdWs heterostructure ferroelectric tunneling junction based on $MoTe_2$ was constructed, which facilitates the exploration of 2D ferroelectric materials application at the memory devices. Weston *et al.* [128] found that mono- or few-layer MoS_2 can assemble ferroelectric semiconductor at room temperature. A twist-controlled network can be arranged into the ferroelectric domains with alternating OOP polarization due to the asymmetry of atomic arrangement at the interface. By applying OOP electrical fields, the ferroelectric domains can be moved. Moreover, Han *et al.* [129] reported 2D Bi_2TeO_5 grown by chemical vapor deposition (CVD) which exhibited the intrinsic IP room temperature ferroelectricity, and the spontaneous polarization arises from Bi column displacement.

Monolayer group-IV monochalcogenides MX (M=Ge, Sn; X=S, Se) with IP electrical polarization and ferroelectricity have robust ferroelectricity and higher corresponding Curie temperatures than room temperature, making them possible for achieving ultrathin ferroelectric devices [130, 131]. Higashitarumizu *et al.* [132] reported that by precisely controlling the growth temperature and pressure in physical vapor deposition (PVD), micron-sized monolayers of SnS can be grown, which opens up the possibility for offering versatility in SnS-based devices. Based on these enlightening works, Lu *et al.* [133] constructed a memristor device based on Ag/SnS/Pt, which has large on/off ratio (10^8), low switching voltage (0.2 V), fast switching speed (1.5 ns), and high reliability. Their work expresses great promise for neuromorphic devices. In addition, SnSe, which belongs to the same family, has also been shown to have excellent ferroelectric properties at room temperature [134, 135].

3.5 Synthesis strategies of 2D ferroelectric materials

For the convenience of the application in memristor and in consideration of the device integration in the future, the best form of prepared 2D ferroelectric materials should be nanosheet and film. In this section, the synthesis strategies of 2D ferroelectric materials in the form of nanosheet and film, including mechanical exfoliation, pulsed laser deposition (PLD), CVD, PVD and liquid phase exfoliation, are introduced and discussed briefly.

Among the various kinds of the synthesis strategies, the mechanical exfoliation method is one of the most prevalent approaches for preparing 2D materials [136, 137] [Fig. 4(a)]. The method was first developed to prepare graphene in 2004 [138]. In recent years, the field of synthesizing large-scale and high-quality 2D ferroelectric materials has made great progress. PLD is a relatively new technology that uses a high energy laser beam as a heating source to bombard the materials to be evaporated, then depositing onto different substrates to prepare thin films [Fig. 4(b)]. CVD is a mature synthesis method; it adopts one or several gas-phase compounds or monomers containing thin film elements as reactants to form thin film on the surface of substrate through a chemical reaction under a relatively high temperature [Fig. 4(c)]. Another mature synthesis method is PVD, which is a technique for depositing thin films through a physical mechanism [Fig. 4(d)].

In addition to the synthesis methods described above, an important factor in the industrial application of 2D ferroelectric materials may be the efficient preparation of high-quality films at low cost and in a simple process. Hence the creation of liquid phase exfoliation, which can be mainly divided into physical and chemical liquid phase exfoliation [Figs. 4(e–g)] [139]. The former can obtain single or few layers of 2D materials directly by sonication. The latter involves the heterogeneous components which can be intercalated into 2D materials by chemical/electrochemical methods to obtain single-layer 2D materials efficiently [140–144].

Some advantages and disadvantages of synthesis strategies based on above are briefly summarized in Table 1.

4 Memristor with 2D ferroelectric materials

Since the discovery of graphene, interest in 2D materials has continued to grow, and their excellent physical properties have made them stand out among the many next-generation information technology materials. The emergence of 2D ferroelectric materials provides more possibilities for developing high performance memristors. Moreover, some 2D ferroelectric materials, for example, α-In_2Se_3 and $CuInP_2S_6$ can further improve the device performance by building vdWs heterostructures for tuning correlated physical properties [154, 165].

2D ferroelectric materials have excellent electrical, optical, thermal, and mechanical properties performances due to atomic-level thickness, which makes them have wide applications in memristors. In the majority of 2D ferroelectric materials, the RS behaviors are related to the ferroelectric domain switching [166–168]. In 2D ferroelectric materials, the controlled ferroelectric domain switching properties in α-In_2Se_3 have been extensively studied to determine the feasibility of memristive and neuromorphic applications [88, 169]. Gabel and Gu [113] constructed a planar ferroelectric memristor based α-In_2Se_3 [Fig. 5(a)], which exhibits two types of

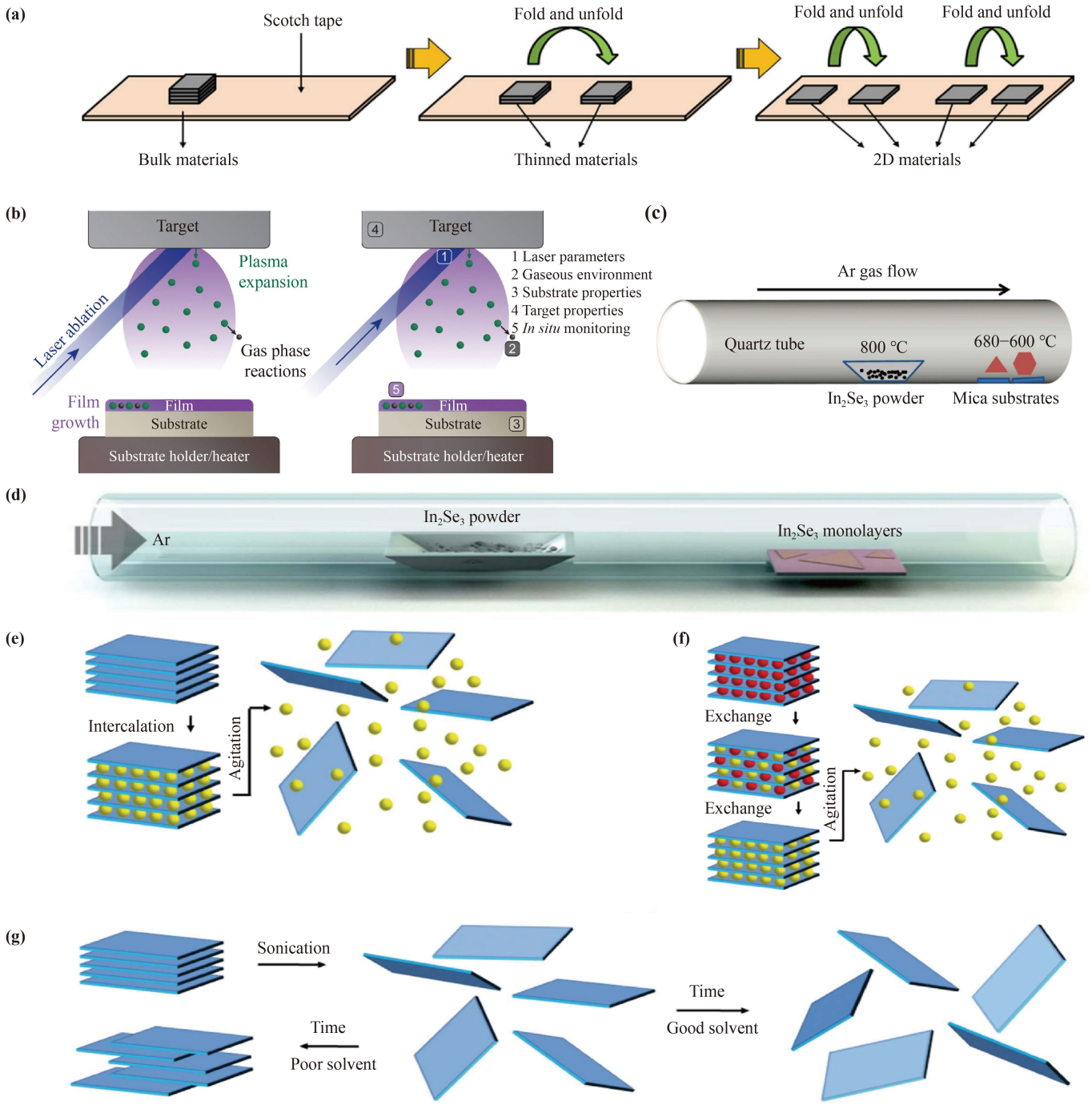

Fig. 4 **(a)** Schematic diagram of mechanical exfoliation process for the production of 2D materials. **(b)** Diagram of the key process and main parameters tailored for use in PLD. **(c)** Schematic diagram of the CVD growth process of 2D ferroelectric material In_2Se_3 on mica substrate. **(d)** In_2Se_3 layers synthesized via PVD with In_2Se_3 powders as precursors. **(e–g)** Schematic diagram of the main liquid exfoliation mechanisms. (a) Reprinted with permission from Ref. [145], Copyright © 2019 The Author(s). Published by Elsevier Ltd. (b) Reprinted with permission from Ref. [146], Copyright © 2023 The Royal Society of Chemistry. (c) Reprinted with permission from Ref. [147], Copyright © 2021 Elsevier B.V. All rights reserved. (d) Reprinted with permission from Ref. [148], Copyright © 2015 American Chemical Society. (e–g) Reprinted with permission from Ref. [139], Copyright © 2013, American Association for the Advancement of Science.

current–voltage relationships: symmetric and rectifying [Figs. 5(b) and (c)], and revealed the formation of energy barriers between ferroelectric domains is the cause of device RS through relevant PFM and Kelvin probe force microscopy (KPFM) studies. To gain microscopic insight into the behaviors of memristive switching,

Table 1 A summary of synthesis strategies to organize 2D ferroelectric materials.

Preparation methods	Advantages	Disadvantages	Ref.
Mechanical exfoliation [Fig. 4(a)]	(1) Easy to operate (2) Highly flexible (3) High quality of prepared material samples	(1) Easy to mix in large amounts of impurities (2) Unstable structure (3) Low production efficiency, cannot be industrialized (4) Poor samples controllability	[55, 77, 79, 89, 136, 137, 149–157]
PLD [Fig. 4(b)]	(1) Rapid response and growth (2) Varieties of films can be made (3) Less contamination to the film, can make high purity film (4) Strong orientation and high film resolution (5) Easy to make multi-layer films and heterogeneous films	(1) Large area deposition of materials cannot be achieved (2) Slow average deposition rate (3) Relatively high cost	[85, 145, 158, 146]
CVD [Fig. 4(c)]	(1) Fast film formation speed, can deposit large quantities of uniformly composed films (2) Good wrap-around properties, complex shaped devices can be uniformly coated (3) Good adhesion strength to the substrate (4) Easy to obtain high purity and good crystallinity of the film (5) A flat deposition surface can be obtained	(1) High reaction temperature may cause coarse grains and brittle phases (2) Affect the service life of the machinery (3) Deposition rate is not too high (4) Easy to pollute the environment	[90, 115, 159–163]
PVD [Fig. 4(d)]	(1) Simple principle, easy to operate (2) Uniform and dense film formation (3) Fast deposition rate and high efficiency (4) Low cost (5) Low environmental pollution	(1) Relatively poor adhesion of the film to the substrate (2) Repeatability is less satisfactory (3) Chemical impurities are difficult to remove	[56, 113, 132]
Liquid phase exfoliation [Fig. 4(e)]	(1) Simple process, easy to operate (2) Mild conditions (3) High crystalline quality (4) Low cost (5) Easy to achieve large-scale production	(1) A bit noisy (2) Small sample size (3) Some auxiliary chemical reagents are easy to pollute the environment and human body	[80, 83, 116, 141, 142, 144, 164]

they performed OOP-PFM and KPFM on devices in the HRS and LRS. The rectifying device demonstrates the I–V_{ds} relationships corresponding to the LRS and HRS, respectively [Figs. 5(d) and (g)]. In LRS, the entire device area, including the In_2Se_3-Au interface and the channel region shows uniform polarization orientation [Fig. 5(e)], that is, the device is in the monodomain state. The surface electric potential in the channel region increases significantly due to the polarization flipping, while the change in the interface region is small [Figs. 5(f) and (i)]. When the device is switched to HRS, ferroelectric domains with different polarization orientations occurred [Fig. 5(h)]. The polarization at the In_2Se_3-Au interface remains essentially constant, while significant polarization reversal can be showed in the channel region.

4.1 α-In_2Se_3 based ferroelectric memristors

Ferroelectric materials have been shown to be the promising candidate for developing high-performance nonvolatile memories such as memristors, which play a key role in the hardware implementation of data storage and artificial synapses [150, 152, 170]. Zhang *et al.* [153] constructed memristor with vertical crossover structure by using α-In_2Se_3 [Fig. 6(a)]. The α-In_2Se_3 nanosheet was obtained by mechanical exfoliation, and a 3 × 6 device array was constructed as shown in Fig. 6(b). Under the voltage sweep, the device shows a hysteresis window at the positive bias part [Fig. 6(c)]. The existence of

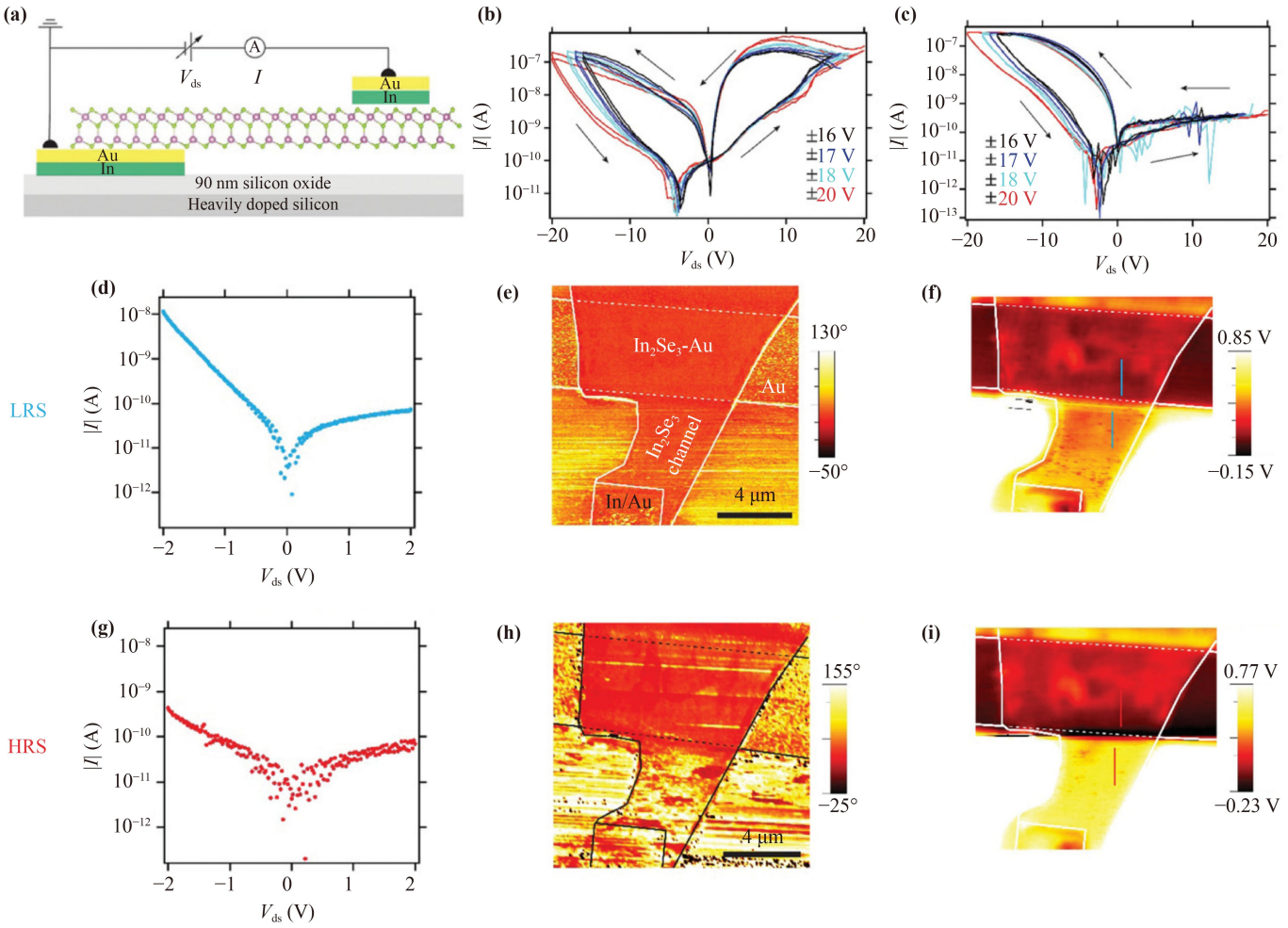

Fig. 5 **(a)** Schematic diagram device structure of α-In_2Se_3 memristor. **(b, c)** Symmetric and rectifying devices with increasing maximum V_{ds}. **(d–f)** $|I|$–V_{ds} relationships, OOP PFM phase images and contact potential difference images of rectifying in the LRS. **(g–i)** $|I|$–V_{ds} relationships, OOP PFM phase images and contact potential difference images of rectifying in the HRS. (a–i) Reprinted with permission from Ref. [113], Copyright © 2020 Wiley-VCH GmbH.

hysteresis window indicates the capability for data storage with the large on/off ratio $>10^3$ (V_{read} = 0.5 V). After 100 cycles of writing (5 V/100 μs) and erasing (–5 V/100 μs), the device performance shows a negligible change [Fig. 6(d)], indicating the excellent endurance. The device also has a good retention, while the on/off ratio can sustain over one order of magnitude for up to 5000 s. The memristor can also be used for mimicking the behaviors of synapse by regarding top and bottom electrodes as pre- and post-synaptic terminals, respectively [Fig. 6(e)]. The long-term potentiation/long-term depression behaviors can be realized by applying a sequence of positive/negative voltage pulses to the pre-synaptic terminal, and the conductance change amplitude increase with the applying pulse intensity [Fig. 6(f)]. By applying two different time spaced voltage pulses to different electrode terminals and recording the changes in synaptic weights, spiking-timing-dependent plasticity (STDP, a temporally asymmetric form of Hebbian learning rules), which is an important learning rule for brain, can be mimicked as shown in [Fig. 6(g)]. Moreover, to verify the feasibility of the device on neuromorphic computing, the α-In_2Se_3 synaptic devices was used to identify the handwritten digit of MNIST dataset by combing ANNs. After training, the neural network based on the real α-In_2Se_3 synaptic device obtained an accuracy of 93.2%, which is not far from that based on ideal hard-based device (94.1%) [Fig. 6(h)].

In Zhang's work [153], the α-In_2Se_3 synaptic device can display either analog or digital memory operations depending on the driving voltage. It can emulate important biological synaptic behaviors through simulating a RS based on Schottky barrier modulation of the ferroelectric polarization. The α-In_2Se_3-based synaptic device with dual mode operation ability has high on/off ratio, good fatigue property, and long retention advantages, which will facilitate the development of high density and complex electronic systems. Wan *et al.* [154] constructed

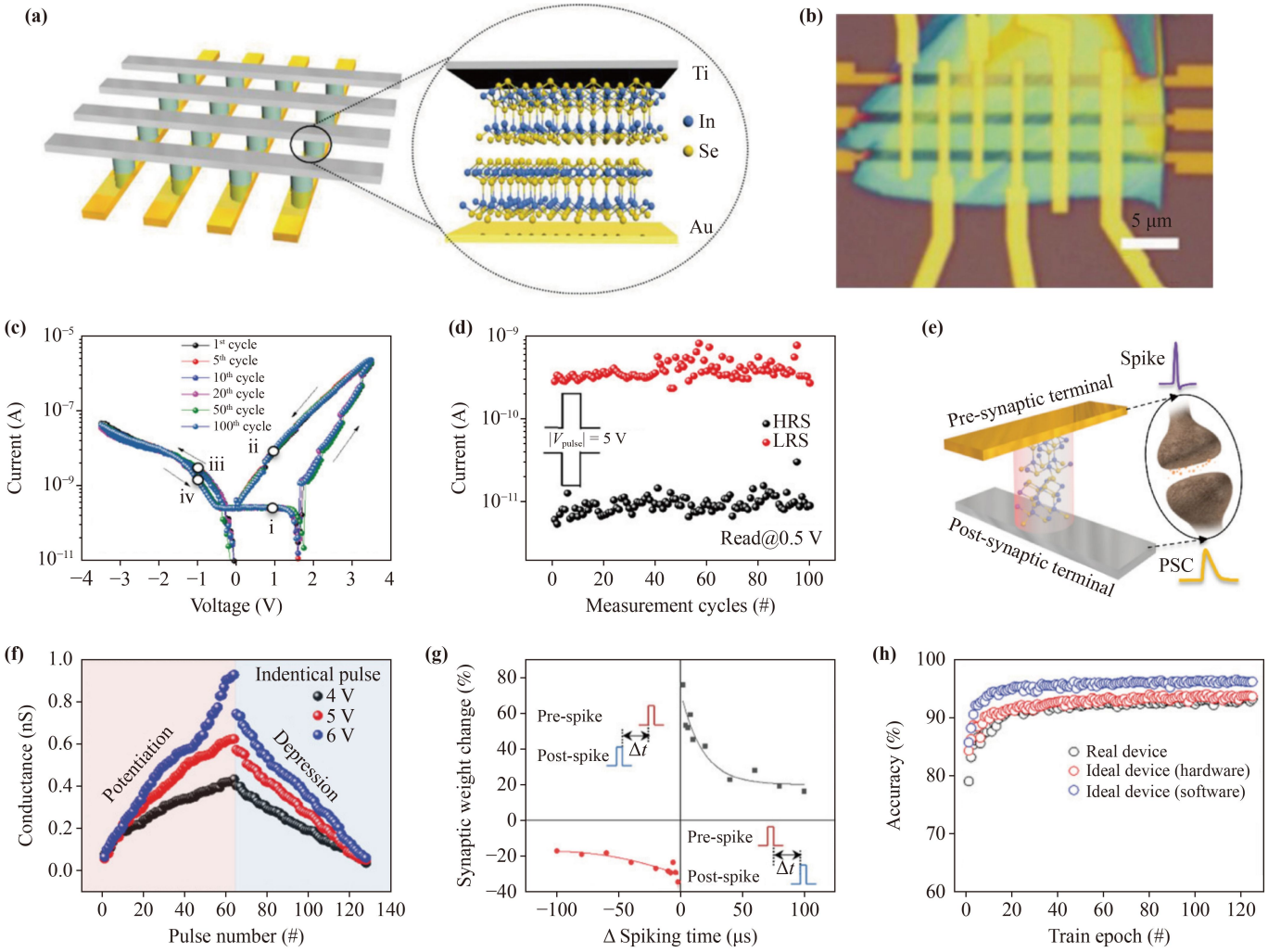

Fig. 6 **(a)** Schematic diagram of α-In_2Se_3-based synaptic device. **(b)** Optical image of the α-In_2Se_3-based synaptic device. **(c)** *I*–*V* curves of the device under voltage sweep. **(d)** The endurance of α-In_2Se_3-based device (100 cycles, set pulse: 5 V/100 μs, reset pulse: –5 V/100 μs). **(e)** Schematic diagram of the artificial synapse based on α-In_2Se_3. **(f)** Long-term potentiation/long-term depression under the different pulse amplitude from 4 to 6 V. The current was read at 0.5 V after each pulse, and the pulse width is fixed with 1 μs. **(g)** STDP learning rules realized by α-In_2Se_3 artificial synapse. **(h)** The recognition results to MNIST handwritten dataset. The recognition accuracy of the α-In_2Se_3-based synaptic device is 93.2%, close to that of based on ideal hard-based device (94.1%). (a–h) Reprinted with permission from Ref. [153], Copyright © 2021 Wiley-VCH GmbH.

a lateral memristor with a transverse β/α/β In_2Se_3 heterojunction structure based on laser writing technique that can trigger the transformation of α-In_2Se_3 to β-In_2Se_3 [Fig. 7(a)]. The unit cells of both α-In_2Se_3 and β-In_2Se_3 crystals are composed of three quintuple layers as shown in Fig. 7(b). Each layer is connected by weak vdWs forces. This asymmetric structure endows the α-phase In_2Se_3 a stable ferroelectricity. Raman spectroscopy can be used to distinguish the α and β phases [Fig. 7(c)]. In the Raman spectrum, a narrow peak located at 104 cm^{-1} is exhibited for the α-phase In_2Se_3, which is recognized as the A (LO + TO) phonon mode, while the 110 cm^{-1} is exhibited for the β phase under the characteristic mode. The device shows a bipolar RS character under the voltage sweep of ±5 V as shown in Fig. 7(d). As shown in Fig. 7(e), two logic states can be encoded by polarizing the α-In_2Se_3, through applying a sequence of periodic pulses of write (+5 V, 10 ms), read (0.1 V, 90 ms), erase (–5 V, 10 ms), and read (0.1 V, 90 ms). The device shows good retention with 1000 s [Fig. 7(f)] and endurance with over 1000 cycles [Fig. 7(g)]. This emerging lateral β/α/β heterojunction memristor with low energy consumption (V_{read} = 0.1 V) can provide a more flexible multi-terminal signal input, and present a tunneling conductance change originating from the IP electric polarization flipping, which expands the device capability greatly.

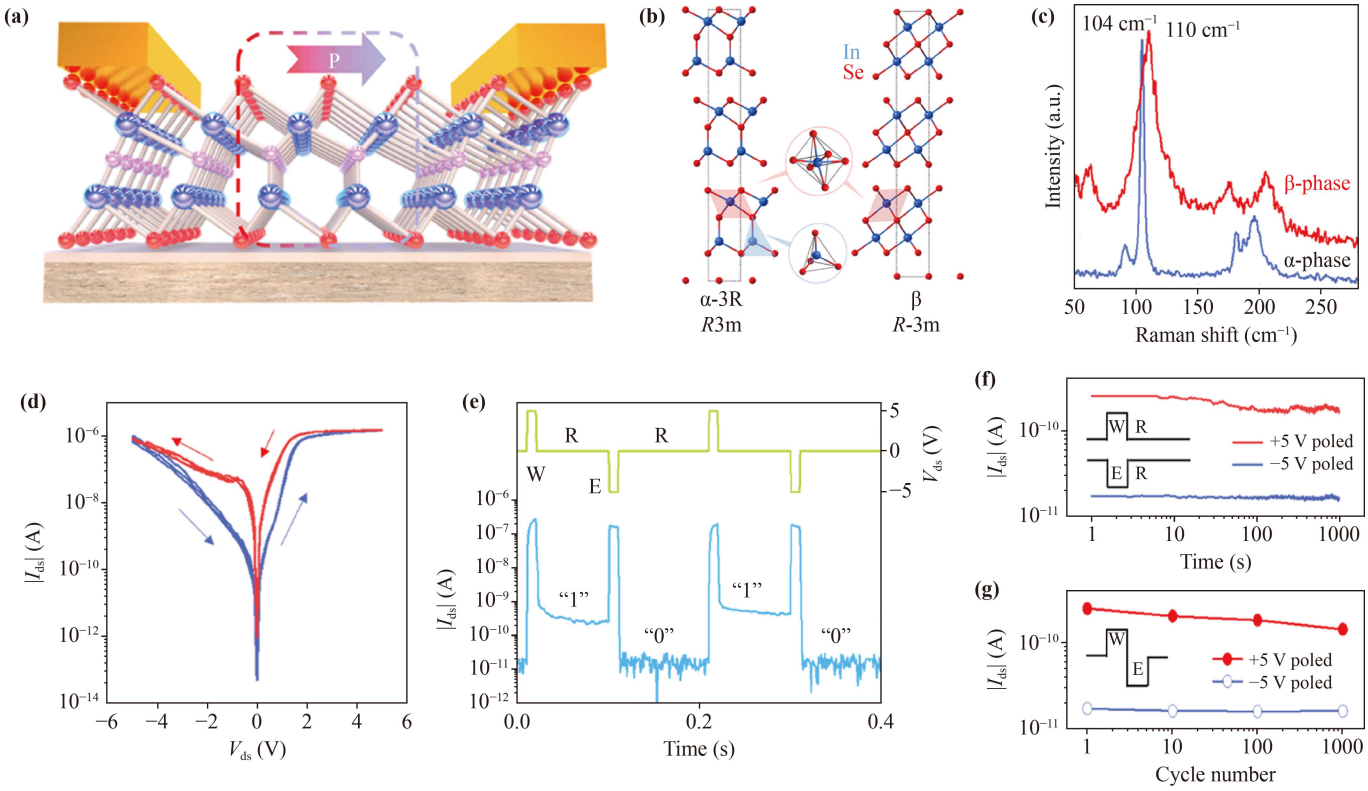

Fig. 7 Nonvolatile ferroelectric memory based on lateral β/α/β In_2Se_3 heterojunction. **(a)** Schematic diagram of a β/α/β In_2Se_3 device. The dashed box in the middle represents the α-phase. The β-phase is in contact with the electrodes at both ends. The position of the pink Se atoms in the middle can be used to distinguish between α-In_2Se_3 and β-In_2Se_3 (Blue: In atoms). The arrows represent the direction of polarization. **(b)** Side view of the cell unit for the α and β of In_2Se_3. Indium (blue balls) and selenium (red balls) atoms combine to form the tetrahedral and octahedral structures shown in the inset, respectively. **(c)** Raman spectroscopy of the α and β phases of In_2Se_3. **(d)** The *I*–*V* curves output measured repeatedly between +5 to –5 V, with the arrows representing the scanning direction. **(e)** The current response under periodic voltage pulses. The pulse width for write and erase is 10 ms, and two logic states can be read at 0.1 V. **(f, g)** The retention and endurance performance of the device. (a–g) Reprinted with permission from Ref. [154], Copyright © 2022 American Chemical Society.

4.2 CIPS based ferroelectric memristors

There are also some studies on 2D CIPS based memristors for data storage and artificial synapses [155, 156]. Utilizing the adjustable characteristic of electrical conductivity in CIPS under electric field, Chen *et al.* [122] constructed a 2D CIPS based artificial synaptic device as shown in Fig. 8(a). Under the electric field, Cu^+ ions will migrate along the field and accumulate at the cathode, so that there will be Cu^+ vacancies near the anode electrode. The inhomogeneous distribution of Cu^+ ions and Cu^+ vacancies can adjust the electrical conductivity, opening up the possibility for the simulation of synaptic behaviors. In order to prove the working mechanism, the *I*–*V* curves after the voltage incentive with different intensities were tested [Fig. 8(b)]. After the incentive, the device shows typical rectification characteristics, and the rectification ratio shows a positive correlation with incentive intensity, indicating more Cu^+ ions can migrate to the cathode due to the larger IP electric field, which may contribute to the conductance and induce the doping of holes and electrons. The device shows an obvious hysteresis with on/off ratio of 20 (V_{read} = 2 V) under the voltage sweep, which promotes the application in neuromorphic device [Fig. 8(c)]. The memristor also has the good retention with 3500 s [Fig. 8(d)] and endurance with 100 cycles characteristics [Fig. 8(e)]. This CIPS device can also be used to mimic the synaptic behaviors, such as paired-pulse facilitation (PPF) [Fig. 8(f)], which can be defined as when two consecutive excitatory stimuli (Δt) from the presynaptic neuron reach the postsynaptic neuron, an enhanced excitatory postsynaptic current response is obtained on the first one. In the brain, the strength of synaptic connections is called synaptic weight. Neural activity can change synaptic weights, called synaptic plasticity, which is the basis for learning and memory in the biological nervous system. Synaptic plasticity is divided into short-term plasticity (STP) and long-term plasticity (LTP) depending on the postsynaptic currents (PSCs). This device can also mimic the synaptic

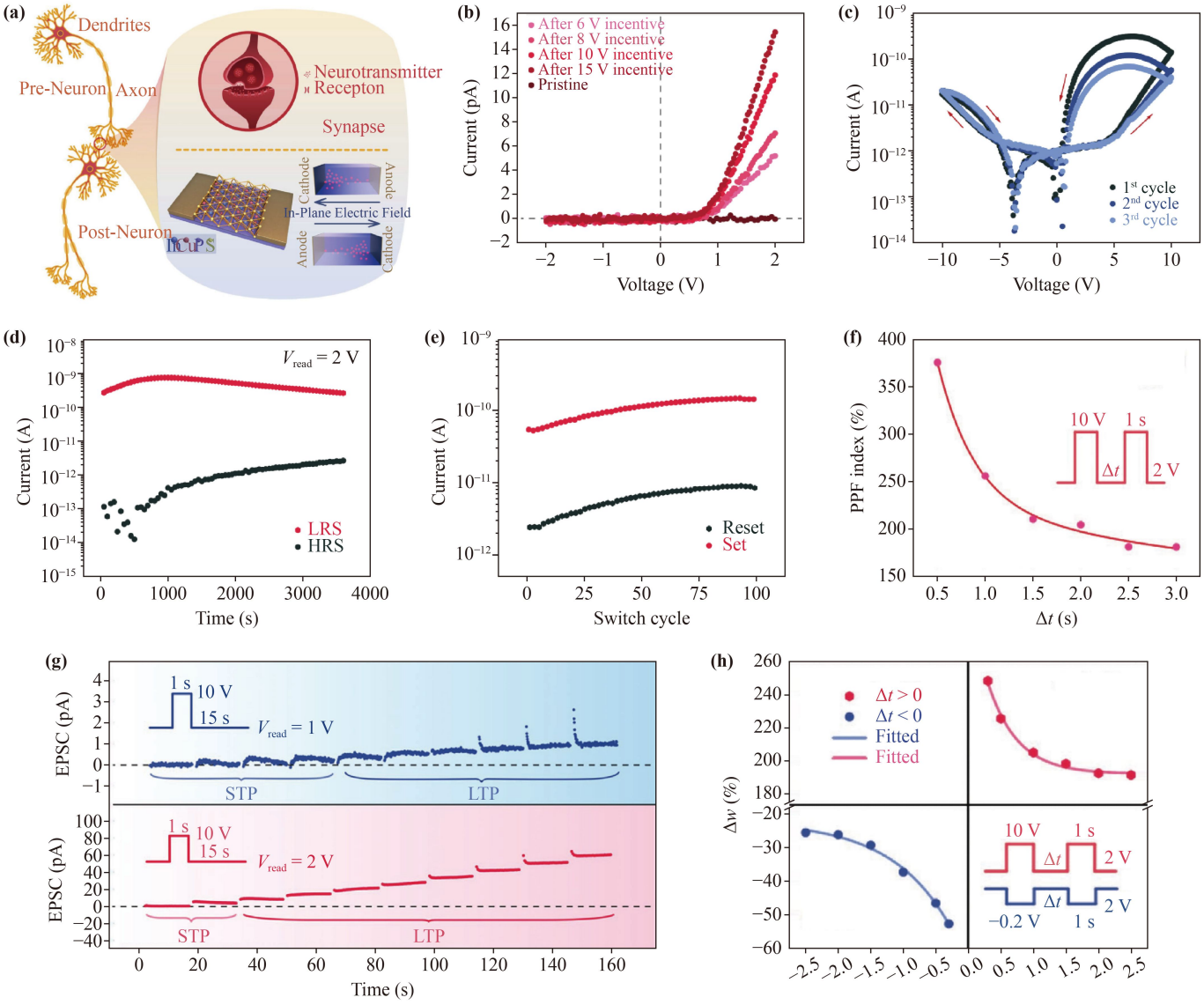

Fig. 8 The mimicking neuroplasticity via Cu^+ ions migration in layered $CuInP_2S_6$. **(a)** Schematic diagram of a biological synapse. The lower right part is the CIPS artificial synaptic device. **(b)** Plot of I–V curves measured at a fixed voltage range (–2 to 2 V) after a voltage sweep from 0 V to positive stimulation voltages (6, 8, 10, 15 V). **(c)** I–V characteristics of the device at a swept voltage range (–10 to 10 V). The light blue, dark blue and black curves indicate the I–V curves for three consecutive cycles of testing, respectively, and the arrows indicate the direction of scanning. **(d)** Current at different resistive states of the device read with a voltage of 2 V after the 10 and –10 V scanning. **(e)** RS stability of the device at a set voltage of 15 V and a reset voltage of –10 V with a V_{read} of 2 V. **(f)** Excitatory postsynaptic currents at different V_{read} after application of a series of 10 V pulses lasting 1 s. **(g)** PPF on the device triggered by a pair of positively spaced pulses with different intervals. **(h)** Implementation of STDP based on CIPS devices with exponential functions fitted to the data points. (a–h) Reprinted with permission from Ref. [122], Copyright © 2021 Wiley-VCH GmbH.

behavior transition from STP to LTP [Fig. 8(g)]. It can infer that the correlated relaxation voltage relating to build-in electric field through the observed transition behaviors from STP to LTP may be slightly less than 2 V. Cu^+ ions partly relax to the origin lattice under 1 V, therefore, compared to the case of V_{read} = 2 V, establishing a similar Cu^+ ions distribution scenario needs a longer duration time of 10 V pulse stimulus in the case of V_{read} = 1 V. In addition, the device can also simulate STDP [Fig. 8(h)]. By constructing a CIPS-based electronic synaptic device and controlling the migration of Cu^+ ions to regulate the electrical conductivity, various biological synaptic functions were successfully simulated. Compared with the above CIPS device with V_{read} = 2 V, the device reading voltage based on the heterojunction structure of CIPS can even be as low as 0.5 V, which can optimize the functionality of the material and reduce the power consumption of the

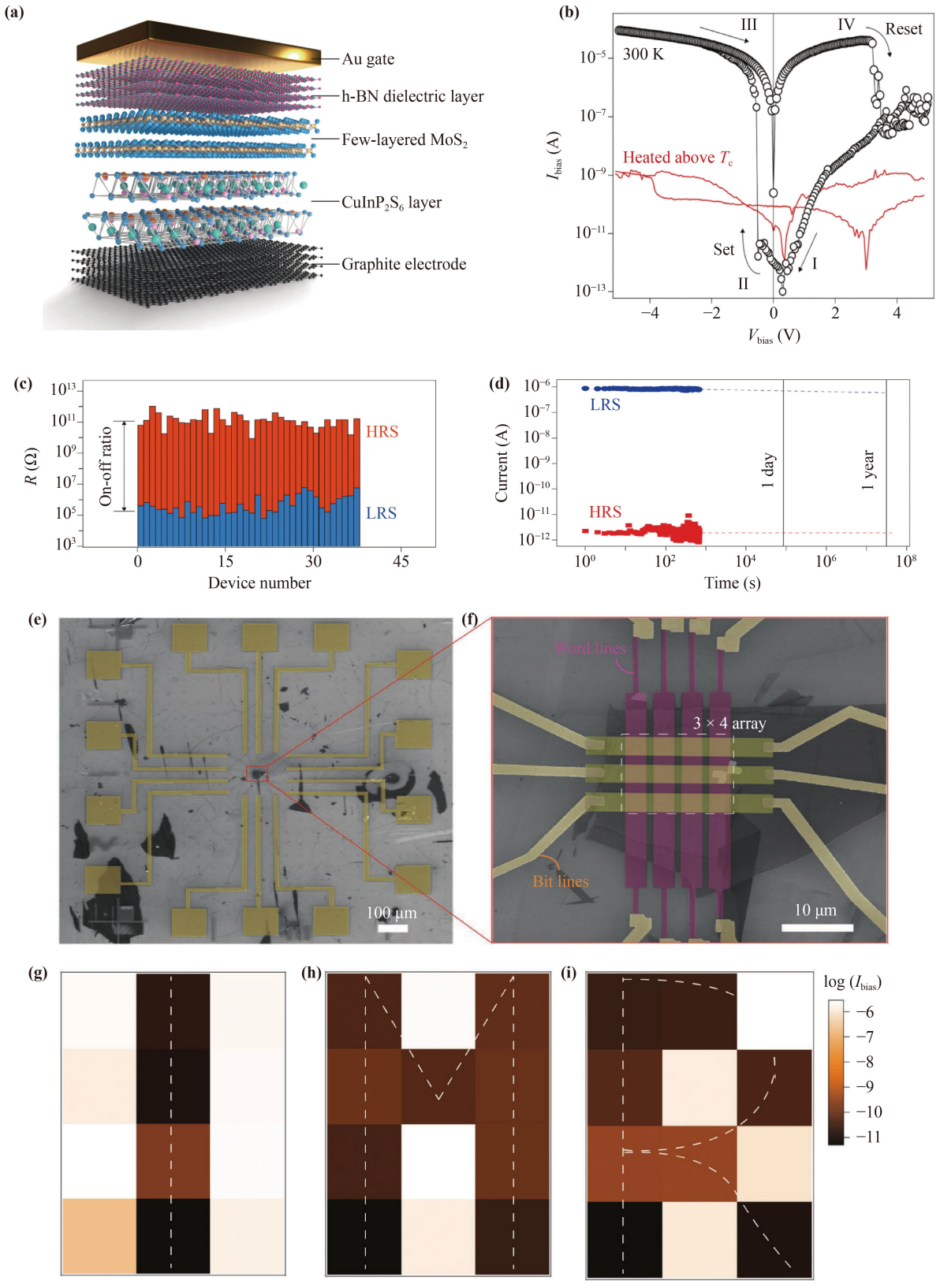

Fig. 9 Gate programmable vertical M–FE–S heterojunction memristor. **(a)** Schematic diagram of the M–FE–S memristor. **(b)** *I*–*V* curves of the M–FE–S memristor under 300 K (room temperature, black) and above T_c 400 K (red). The arrows indicate the scanning direction. **(c, d)** Reproducibility and retention. **(e, f)** SEM images of a 3 × 4 M–FE–S array device. **(g–i)** The letters "I", "M" and "R" encoded by reading the HRS and LRS of each pixel in the 3 × 4 array. (a–i) Reprinted with permission from Ref. [171], Copyright © 2022 The Authors. Advanced Materials published by Wiley-VCH GmbH.

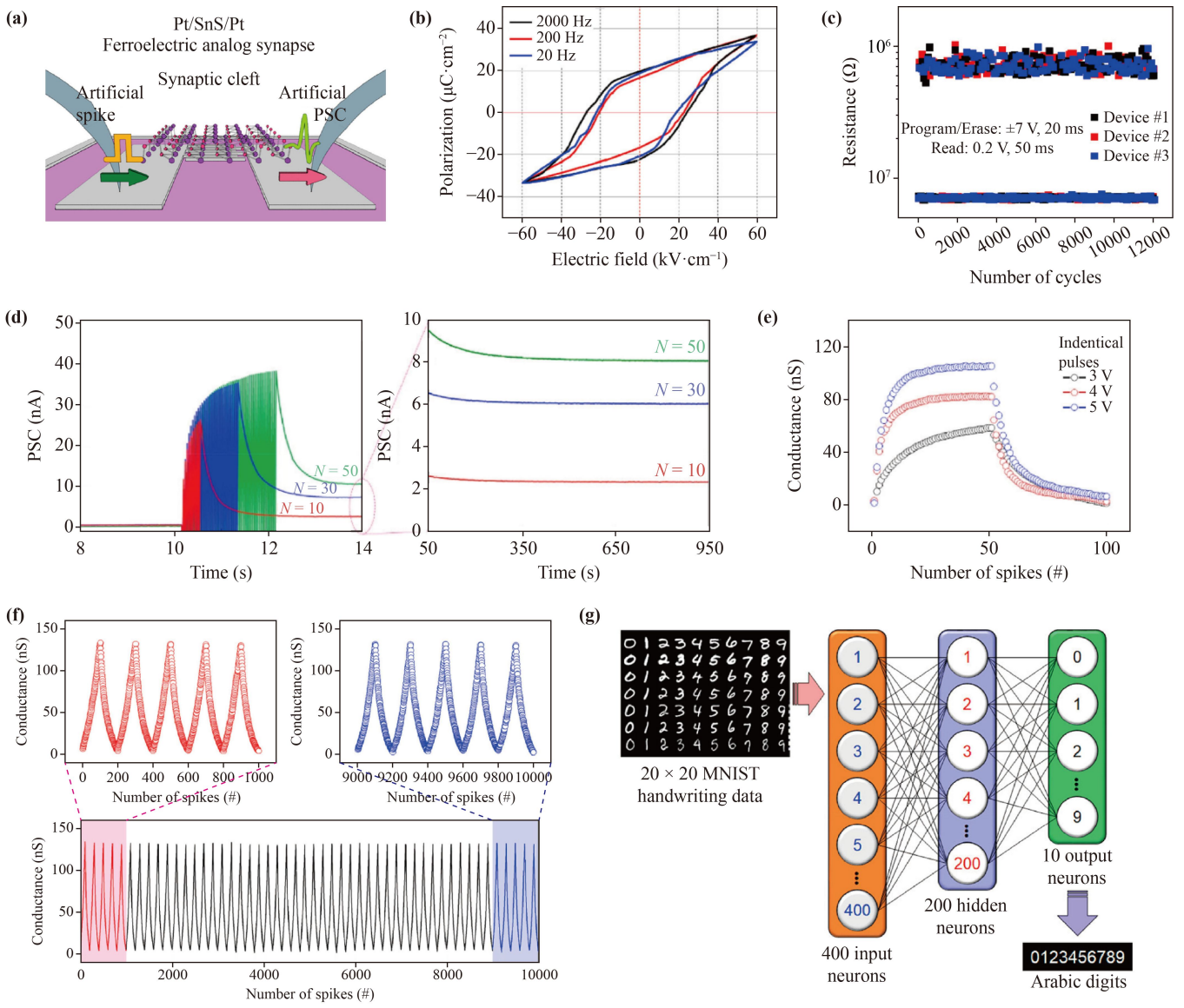

Fig. 10 **(a)** Schematic diagram of the Pt/SnS/Pt synapse structure. **(b)** SnS polarization-electric field (P–E) hysteresis curve. **(c)** The performance of fatigue resistance and stability in 3 different devices. **(d)** PPF performance stimulated by applying 10, 30, and 50 presynaptic spikes ($V_{\text{pulse}} = 3$ V, $P_{\text{width}} = 20$ ms), read at 0.1 V. **(e)** LTP/LTD under different pulse amplitude (±3 V to ±5 V). Pulses width: 20 ms. **(f)** Cyclic LTP/LDP tests of this Pt/SnS/Pt artificial synapse. **(g)** The diagram of ANNs for the recognition of handwriting Arabic digits. (a–g) Reprinted with permission from Ref. [159], Copyright © 2020 American Chemical Society.

device [157, 171, 172].

Recently, Li *et al.* [171] constructed a memristor with metal (M)–ferroelectric (FE)–semiconductor (S) architecture based on graphite, CIPS and MoS_2 as shown in Fig. 9(a). The device shows a typical bipolar RS characteristic with a high on/off ratio (10^5) [Fig. 9(b)], moreover, when the same device is heated at 400 K, the RS is quenched since the T_c of $CuInP_2S_6$ studied is ≈ 315 K. The memristor demonstrates good reproducibility [Fig. 9(c)] and excellent retention [Fig. 9(d)]. To investigate the high stability of the memristors based on M–FE–S, a typical of 3 × 4 cross-bar M–FE–S array device is constructed as shown in Figs. 9(e) and (f). The pattern writing process is achieved by programming the corresponding M–FE–S devices in the array with a 100 ms wide polarization voltage $V_{\text{pole}} \approx \pm 4$ V pulses into a potentiation (LRS) or a depression (HRS). The memorized letters can then be read under a bias voltage of 1 V, and the example letters "I", "M", and "R" encoded as 3 × 4-pixel images are stored, as shown in Figs. 9(g–i). The device exhibits two-terminal switchable resistance with on/off ratio over 10^5 and long-term retention. In addition, the carriers concentration of the semiconductor layer MoS_2 can be modulated to achieve gate

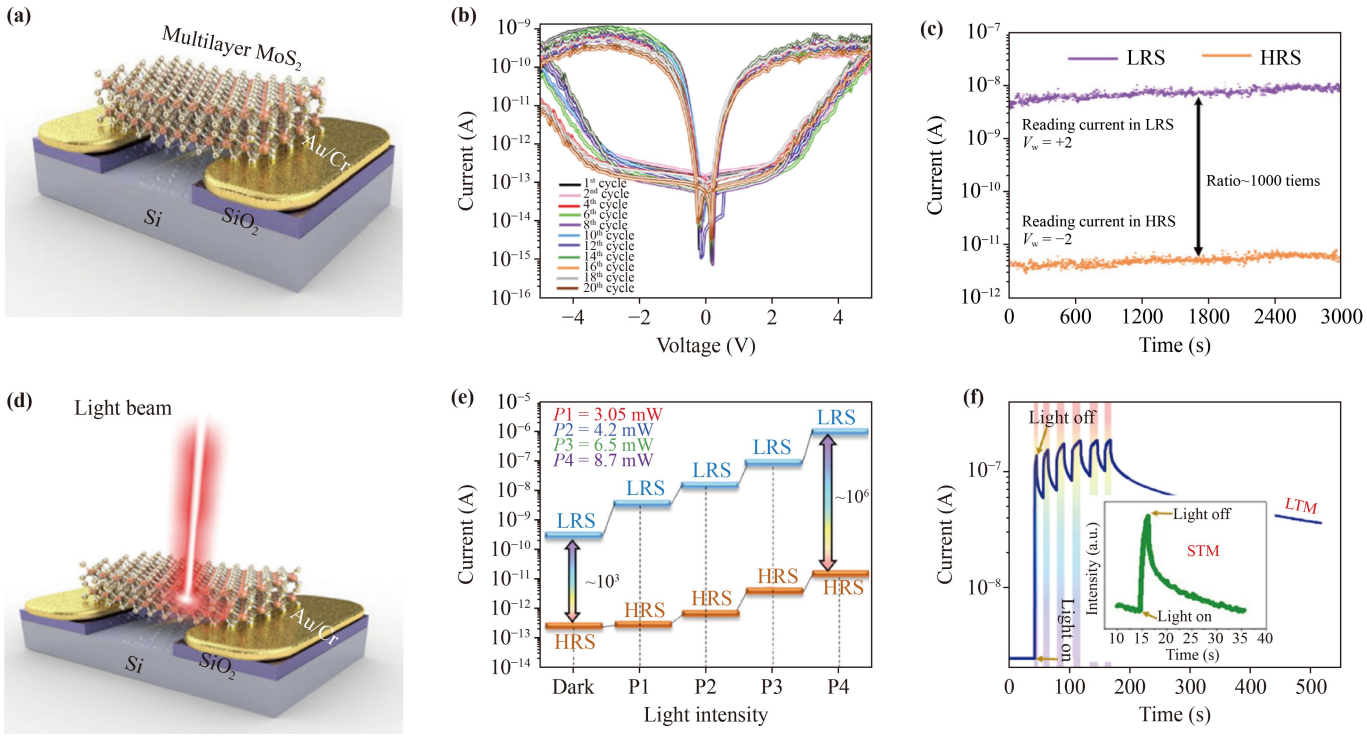

Fig. 11 **(a)** Schematic diagram of a multilayer MoS_2 device consisting of two Cr/Au electrodes. **(b)** *I*–*V* characteristics of the multilayer MoS_2 over 20 cycles, showing excellent stability. **(c)** HRS and LRS currents retention test over 3000 s. **(d)** Schematic illustration of the multilayer MoS_2 device under light illumination. **(e)** The ratio of LRS to HRS changes after light modulation at different power levels, leading to a maximum ratio of 10^5. **(f)** After six consecutive light pulses at 1 V bias, the device transitions to long-term memory (LTM) mode (the inset shows that after a single light pulse at 2 mW power, the short-term memory (STM) mode). (a–f) Reprinted with permission from Ref. [173], Copyright © 2021 American Chemical Society.

programmable RS behaviors in the devices. This study constructs a 2D ferroelectric memristor with vertical heterojunction and a programmable gate voltage, laying the foundation for the application of ferroelectric-mediated memories in 2D nanoelectronics.

4.3 Ferroelectric memristors of other 2D ferroelectric materials

With the in-depth study, more and more 2D materials have been found to be ferroelectric proved by experiment or calculation, such as $Ti_3C_2T_x$ MXene [126], $MoTe_2$ [56], and MoS_2 [173]. Tahir *et al.* [126] reported the ferroelectricity of 2D $Ti_3C_2T_x$ MXene films at room temperature. The presence of defective TiO_2 phases and defects in the Ti-C layer of MXene by heat treatment results in ferroelectric properties of $Ti_3C_2T_x$ MXene, which can be used the application for data storage. However, $Ti_3C_2T_x$ based memristors suffer from the challenges of current abrupt switching. In order to overcome those challenges, Wang *et al.* [174] proposed a strategy to remove the current abrupt behavior and improve the performance of $Ti_3C_2T_x$ based memristors by doping Mxenes with Ag nanoparticle, which provides a reference for the application of MXenes in ferroelectric neuromorphic devices.

Kwon *et al.* [159] prepared a Pt/SnS/Pt-based artificial synapse as shown in Fig. 10(a). The *P*–*E* curves [Fig. 10(b)] show an obvious hysteresis loop. The sweeping frequency increases from 20 Hz to 2000 Hz and the coercive field increases slightly to a higher value. The devices keep stable and show little difference during the continuous stimulations of program/erase operation with 10^4 cycles [Fig. 10(c)], indicating the excellent fatigue resistance and stability, which are considered as one of the most important features of artificial synapse. PPF was successfully performed by adjusting the number and the time interval of pulses applied to the device. The results show an increase in synaptic strength with the pulse number and decrease of pulse time intervals [Fig. 10(d)]. The device can also realize LTP/LTD behaviors by applying the same successive enhancement/inhibition pulse trains with different amplitudes (±3 V to ±5 V) to presynaptic neurons, and it was found that higher PSCs could be collected under larger pulse amplitudes [Fig. 10(e)]. The device also has a stable enhancement/inhibition behavior with 50 cycles under 10^4 pulses [Fig. 10(f)]. Finally, based on the supervised ANNs, the device achieves 92.1% accuracy during the recognition task for the images of handwriting Arabic digits [Fig. 10(g)].

In 2017, Li *et al.* [92] reported the 2D vertical ferroelectricity with first-principles evidence induced by interlayer translation, which is widely present in graphite bilayers of BN, AlN, ZnO, MoS_2, GaSe, etc. In theory, MoS_2-based devices can have a larger current on/off ratio ($>10^{10}$) and an ideal sub-threshold swing (60 mV·dec^{-1}), and it is unaffected by short-channel effects [175]. In addition, strong photoluminescence has been detected in monolayer MoS_2 [176]. These excellent electronic and optical properties make ultrathin MoS_2 promising for low energy consumption optoelectronic applications. For example, Abnavi *et al.* [173] reported a structure with multilayer MoS_2 flakes and a bridge-like pattern over two Cr/Au electrodes [Fig. 11(a)]. The *I*–*V* (–5 to 5 V) characteristics of the device for 20 continuous cycles are shown in Fig. 11(b), indicating that the device still maintains the LRS and HRS transition over 20 cycles. The device also has a stable retention for at least 3000 s and a high current on/off ratio of ~10^3 [Fig. 11(c)]. To further improve the on/off ratio between the LRS and HRS, a modulated continuous-wave laser beam is used to illuminate the MoS_2 device, as shown in [Fig. 11(d)]. The light was turned on at different voltages at the HRS level, which can result in an abrupt transition to the LRS level due to the production of electron/hole carriers, therefore it is possible to increase the current ratio of the LRS to the HRS to achieve an on/off ratio of up to 10^5 through increasing the power of the laser beam [Fig. 11(e)]. When a single short light pulse is applied to the device, a single peak current is produced due to the photogeneration and the current versus time response is shown in Fig. 11(f). When the light is off, the current slowly decays and does not immediately return to the initial value, which is a well-known phenomenon known as persistent photoconductivity (PPC). PPC in MoS_2 channels is attributed to charge trapping at the sites of oxygen-related defects on the MoS_2 surfaces. This work presents a simple method for the fabrication of reliable RS devices for neuromorphic applications.

Previous studies have mostly investigated the ferroelectricity of SnTe monolayers and their ferroelectric critical size [177], and research on ferroelectricity of SnTe has been carried out since 2016 [61]. It should be noted that the vortex in their interaction is actually a vortex-like arrangement of atoms, and this is a collective atomic motion, which can also be controlled. This is a new physical phenomenon that can be used to develop high performance device [64], However, the related application study has not appeared yet.

5 Summary and outlook

The high energy consumption and low processing efficiency resulted from von Neuman bottleneck promote the development of a brain-like device with parallelism, low power consumption, and high processing efficiency. 2D ferroelectric materials have become a hot research topic in the field of memristors because of their stable ferroelectricity at room temperature, good stability at ultrathin scales, and reversible polarization direction under the external action factors. In addition, the property of interlayer slip ferroelectricity has further enriched the applications of 2D ferroelectric materials, such as memristors.

In this review, we first briefly introduce the basic physical properties of the 2D ferroelectric materials, such as excellent piezoelectricity, ferroelectricity, and pyroelectric effect. Then, several representative 2D ferroelectric materials are introduced, and the common synthetic methods are summarized for comparing their advantages and disadvantages. At last, the application of 2D ferroelectric materials in memristors are discussed.

Although ferroelectric materials have been developed for about a hundred years, research about 2D ferroelectric materials, especially the application in memristor is still at an early stage. Further efforts are needed to improve material and device performance. (i) The dipole polarization of 2D ferroelectric materials is the foundation of their most electrical properties, but the complete dynamics of reversible switching at the atomic level is still not fully understood. In this aspect, some new techniques, such as machine learning based potential simulations, can provide a new direction for this research. (ii) Although there are several methods for synthesizing 2D ferroelectric materials, none of them can meet the demands of fast deposition rate, high efficiency, and factory production, simultaneously. Therefore, much efforts are needed to produce the high quality 2D ferroelectric materials with large size, low cost, and high flexibility. (iii) The variability of ferroelectric polarization switching speed of devices is relatively high, even for the same 2D ferroelectric material. In addition, the device reading and writing speed are also affected by certain geometry and test instruments. Therefore, the stability, durability and switching speed of 2D ferroelectric materials, and related test instruments require further improvement. (iv) For different 2D ferroelectric materials, some have OOP or IP ferroelectricity, and some have both. Therefore, it is necessary to explore comprehensively the ferroelectricity in OOP and IP. (v) At present, most studies about 2D ferroelectric material-based memristors are based on single device and still in the laboratory level, large-scale device array and integration are needed for future practical application. (vi) Currently, the applications of 2D ferroelectric material based memristors focus on the initial stage, but the applications in artificial synapses and neurons also have tremendous advantages. Therefore, there is an urgent need to expand the application of 2D ferroelectric material based memristors. (vii) Compared to the pristine 2D ferroelectric materials, the heterojunction structures

based memristor are infrequently reported. The heterojunction structure based on 2D ferroelectric materials can show higher performance than pristine materials in on/off ratio and energy consumption. Therefore, 2D ferroelectric heterojunction memristors need to be studied in depth. (viii) Now, single-layer 2D materials can be fabricated through various preparation methods, but it is difficult to prepare the continuous multilayer heterojunctions because the growth of a continuous multilayer tends to destroy the properties and quality of the underlying material. Therefore, the multilayer and large-area heterostructures preparations which have the controllable and continuous characteristics are a potential area for future development. (ix) In addition, new device structure designs, circuit designs, and compatibility with complementary metal oxide semiconductor circuits are less mature, so they are all likely to become research hotspots in the future.

Declarations The authors declare that they have no competing interests and there are no conflicts.

Acknowledgements We acknowledge grants from the National Natural Science Foundation of China (Grant No. 61974093), the Guangdong Basic and Applied Basic Research Foundation (Grant No. 2023A1515012479), the Science and Technology Innovation Commission of Shenzhen (Grant Nos. RCYX20200714114524157 and JCYJ20220818100206013), and the NTUT-SZU Joint Research Program (Grant No. NTUT-SZU-112-02).

References

1. J. Ajayan, D. Nirmal, B. K. Jebalin I. V, and S. Sreejith, Advances in neuromorphic devices for the hardware implementation of neuromorphic computing systems for future artificial intelligence applications: A critical review, *Microelectron. J.* 130, 105634 (2022)
2. B. Sun, S. Ranjan, G. Zhou, T. Guo, Y. Xia, L. Wei, Y. N. Zhou, and Y. A. Wu, Multistate resistive switching behaviors for neuromorphic computing in memristor, *Mater. Today Adv.* 9, 100125 (2021)
3. K. Sun, J. Chen, and X. Yan, The future of memristors: Materials engineering and neural networks, *Adv. Funct. Mater.* 31(8), 2006773 (2021)
4. D. Misra, Special issue of Interface on Neuromorphic Computing: An introduction and state of the field, *Electrochem. Soc. Interface* 32(1), 45 (2023)
5. D. Ielmini, Z. Wang, and Y. Liu, Brain-inspired computing via memory device physics, *APL Mater.* 9(5), 050702 (2021)
6. J. Q. Yang, R. Wang, Y. Ren, J. Y. Mao, Z. P. Wang, Y. Zhou, and S. T. Han, Neuromorphic engineering: From biological to spike-based hardware nervous systems, *Adv. Mater.* 32(52), 2003610 (2020)
7. L. Wang, X. Shen, Z. Gao, J. Fu, S. Yao, L. Cheng, and X. Lian, Review of applications of 2D materials in memristive neuromorphic circuits, *J. Mater. Sci.* 57(8), 4915 (2022)
8. Z. Wang, L. Wang, M. Nagai, L. Xie, M. Yi, and W. Huang, Nanoionics-enabled memristive devices: Strategies and materials for neuromorphic applications, *Adv. Electron. Mater.* 3(7), 1600510 (2017)
9. C. Gao, M. P. Lee, M. Li, K. C. Lee, F. S. Yang, C. Y. Lin, K. Watanabe, T. Taniguchi, P. W. Chiu, C. H. Lien, W. W. Wu, S. P. Lin, W. Li, Y. F. Lin, and J. Chu, Mimic drug dosage modulation for neuroplasticity based on charge-trap layered electronics, *Adv. Funct. Mater.* 31(5), 2005182 (2021)
10. X. Wang, Z. Shang, C. Zhang, J. Kang, T. Liu, X. Wang, S. Chen, H. Liu, W. Tang, Y. J. Zeng, J. Guo, Z. Cheng, L. Liu, D. Pan, S. Tong, B. Wu, Y. Xie, G. Wang, J. Deng, T. Zhai, H. X. Deng, J. Hong, and J. Zhao, Electrical and magnetic anisotropies in van der Waals multiferroic $CuCrP_2S_6$, *Nat. Commun.* 14(1), 840 (2023)
11. R. Lin, G. Shi, F. Qiao, C. Wang, and S. Wu, Research progress and applications of memristor emulator circuits, *Microelectron. J.* 133, 105702 (2023)
12. Y. Zuo, H. Lin, J. Guo, Y. Yuan, H. He, Y. Li, Y. Xiao, X. Li, K. Zhu, T. Wang, X. Jing, C. Wen, and M. Lanza, Effect of the pressure exerted by probe station tips in the electrical characteristics of memristors, *Adv. Electron. Mater.* 6(3), 1901226 (2020)
13. O. Vaughan, A history of memristors in five covers, *Nat. Electron.* 6(1), 7 (2023)
14. L. Chua, Memristor—The missing circuit element, *IEEE Transactions on Circuit Theory* 18(5), 507 (1971)
15. S. Yan, J. Zang, P. Xu, Y. Zhu, G. Li, Q. Chen, Z. Chen, Y. Zhang, M. Tang, and X. Zheng, Recent progress in ferroelectric synapses and their applications, *Sci. China Mater.* 66(3), 877 (2023)
16. W. Chen, L. Song, S. Wang, Z. Zhang, G. Wang, G. Hu, and S. Gao, Essential characteristics of memristors for neuromorphic computing, *Adv. Electron. Mater.* 9(2), 2200833 (2022)
17. S. H. Sung, Y. Jeong, J. W. Oh, H. J. Shin, J. H. Lee, and K. J. Lee, Bio-plausible memristive neural components towards hardware implementation of brain-like intelligence, *Mater. Today* 62, 251 (2023)
18. F. Yuan and Y. Li, A chaotic circuit constructed by a memristor, a memcapacitor and a meminductor, *Chaos* 29(10), 101101 (2019)
19. Z. Biolek, D. Biolek, V. Biolková, Z. Kolka, A. Ascoli, and R. Tetzlaff, Analysis of memristors with nonlinear memristance versus state maps, *Int. J. Circuit Theory Appl.* 45(11), 1814 (2017)
20. M. Di Ventra, Y. V. Pershin, and L. O. Chua, Circuit elements with memory: Memristors, memcapacitors, and meminductors, *Proc. IEEE* 97(10), 1717 (2009)
21. S. G. Kim, J. S. Han, H. Kim, S. Y. Kim, and H. W. Jang, Recent advances in memristive materials for artificial synapses, *Adv. Mater. Technol.* 3(12), 1800457 (2018)
22. X. Yan, H. Yan, G. Liu, J. Zhao, Z. Zhao, H. Wang, H. He, M. Hao, Z. Li, L. Wang, W. Wang, Z. Jian, J. Li, and J. Chen, Silicon-based epitaxial ferroelectric memristor for high temperature operation in self-

assembled vertically aligned $BaTiO_3$-CeO_2 films, *Nano Res.* 15(10), 9654 (2022)
23. Z. Liu, H. Wang, M. Li, L. Tao, T. R. Paudel, H. Yu, Y. Wang, S. Hong, M. Zhang, Z. Ren, Y. Xie, E. Y. Tsymbal, J. Chen, Z. Zhang, and H. Tian, In-plane charged domain walls with memristive behaviour in a ferroelectric film, *Nature* 613(7945), 656 (2023)
24. X. Yan, X. Jia, Y. Zhang, S. Shi, L. Wang, Y. Shao, Y. Sun, S. Sun, Z. Zhao, J. Zhao, J. Sun, Z. Guo, Z. Guan, Z. Zhang, X. Han, and J. Chen, A low-power Si:HfO_2 ferroelectric tunnel memristor for spiking neural networks, *Nano Energy* 107, 108091 (2023)
25. Y. W. Fang, Z. J. Yang, R. Y. Liao, P. T. Chen, C. B. Liu, K. Y. Huang, H. H. Hsu, C. H. Cheng, W. C. Chou, S. H. Lin, and Y. Zhou, Electrical characteristics investigation of ferroelectric memories using stacked and mixed hafnium zirconium oxides, *Thin Solid Films* 757, 139395 (2022)
26. F. S. Yang, M. Li, M. P. Lee, I. Y. Ho, J. Y. Chen, H. Ling, Y. Li, J. K. Chang, S. H. Yang, Y. M. Chang, K. C. Lee, Y. C. Chou, C. H. Ho, W. Li, C. H. Lien, and Y. F. Lin, Oxidation-boosted charge trapping in ultra-sensitive van der Waals materials for artificial synaptic features, *Nat. Commun.* 11(1), 2972 (2020)
27. L. Yin, R. Cheng, Y. Wen, B. Zhai, J. Jiang, H. Wang, C. Liu, and J. He, High-performance memristors based on ultrathin 2D copper chalcogenides, *Adv. Mater.* 34(9), 2108313 (2022)
28. F. Qian, R. S. Chen, R. Wang, J. Wang, P. Xie, J. Y. Mao, Z. Lv, S. Ye, J. Q. Yang, Z. Wang, Y. Zhou, and S. T. Han, A leaky integrate-and-fire neuron based on hexagonal boron nitride (h-BN) monocrystalline memristor, *IEEE Trans. Electron Dev.* 69(11), 6049 (2022)
29. Z. P. Wang, P. Xie, J. Y. Mao, R. Wang, J. Q. Yang, Z. Feng, Y. Zhou, C. C. Kuo, and S. T. Han, The floating body effect of a WSe_2 transistor with volatile memory performance, *Mater. Horiz.* 9(7), 1878 (2022)
30. Z. Wang, W. Wang, P. Liu, G. Liu, J. Li, J. Zhao, Z. Zhou, J. Wang, Y. Pei, Z. Zhao, J. Li, L. Wang, Z. Jian, Y. Wang, J. Guo, and X. Yan, Superlow power consumption artificial synapses based on WSe_2 quantum dots memristor for neuromorphic computing, *Research* 2022, 9754876 (2022)
31. B. Cheng, Z. Lei, and P. Wu, Bio-derived crystalline silk nanosheets for versatile macroscopic assemblies, *Nano Res.* 15(6), 5538 (2022)
32. W. Lee, Z. Zhou, X. Chen, N. Qin, J. Jiang, K. Liu, M. Liu, T. H. Tao, and W. Li, A rewritable optical storage medium of silk proteins using near-field nano-optics, *Nat. Nanotechnol.* 15(11), 941 (2020)
33. M. Z. Li, L. C. Guo, G. L. Ding, K. Zhou, Z. Y. Xiong, S. T. Han, and Y. Zhou, Inorganic perovskite quantum dot-based strain sensors for data storage and in-sensor computing, *ACS Appl. Mater. Interfaces* 13(26), 30861 (2021)
34. X. F. Cheng, W. H. Qian, J. Wang, C. Yu, J. H. He, H. Li, Q. F. Xu, D. Y. Chen, N. J. Li, and J. M. Lu, Environmentally robust memristor enabled by lead-free double perovskite for high-performance information storage, *Small* 15(49), 1905731 (2019)
35. Q. Liu, W. Yue, Y. Li, W. Wang, L. Xu, Y. Wang, S. Gao, C. Zhang, H. Kan, and C. Li, Multifunctional optoelectronic random access memory device based on surface-plasma-treated inorganic halide perovskite, *Adv. Electron. Mater.* 7(7), 2100366 (2021)
36. X. Zhu, Q. Wang, and W. D. Lu, Memristor networks for real-time neural activity analysis, *Nat. Commun.* 11(1), 2439 (2020)
37. J. Zhao, W. Li, X. Wang, X. Wei, H. Zhu, W. Qu, D. Men, Z. Gao, B. Wei, H. Gao, and Y. Wu, Organic memristor based on high planar cyanostilbene/polymer composite films, *Chem. Res. Chin. Univ.* 39(1), 121 (2023)
38. Z. Feng, M. Comí, Y. Ren, D. Sredojević, S. Attar, J. Yang, Z. Wang, R. S. Chen, S. T. Han, M. Al-Hashimi, and Y. Zhou, Organic memory devices and synaptic simulation based on indacenodithienothiophene (IDTT) copolymers with improved planarity, *J. Mater. Chem. C* 10(43), 16604 (2022)
39. W. Wang, G. Zhou, Y. Wang, B. Yan, B. Sun, S. Duan, and Q. Song, Multiphotoconductance levels of the organic semiconductor of polyimide-based memristor induced by interface charges, *J. Phys. Chem. Lett.* 13(42), 9941 (2022)
40. L. Qi, S. Ruan, and Y. J. Zeng, Review on recent developments in 2D ferroelectrics: Theories and applications, *Adv. Mater.* 33(13), 2005098 (2021)
41. C. Wang, L. You, D. Cobden, and J. Wang, Towards two-dimensional van der Waals ferroelectrics, *Nat. Mater.* 22(5), 542 (2023)
42. J. Wang, J. Lou, J. F. Wang, S. B. Qu, H. L. Du, and T. J. Cui, Ferroelectric composite artificially-structured functional material: Multifield control for tunable functional devices, *J. Phys. D* 55(30), 303002 (2022)
43. C. Yang, C. Wang, and Z. Cheng, Editorial for the special issue "Nanoscale ferroic materials — ferroelectric, piezoelectric, magnetic, and multiferroic materials", *Nanomaterials (Basel)* 12(17), 2951 (2022)
44. L. W. Martin and A. M. Rappe, Thin-film ferroelectric materials and their applications, *Nat. Rev. Mater.* 2(2), 16087 (2016)
45. K. Geirhos, S. Reschke, S. Ghara, S. Krohns, P. Lunkenheimer, and I. Kézsmárki, Optical, dielectric, and magnetoelectric properties of ferroelectric and antiferroelectric lacunar spinels, *Phys. Status Solidi B* 259(5), 2100160 (2022)
46. F. Xue, X. He, W. Liu, D. Periyanagounder, C. Zhang, M. Chen, C. H. Lin, L. Luo, E. Yengel, V. Tung, T. D. Anthopoulos, L. J. Li, J. H. He, and X. Zhang, Optoelectronic ferroelectric domain-wall memories made from a single van der Waals ferroelectric, *Adv. Funct. Mater.* 30(52), 2004206 (2020)
47. J. Nam, H. Lee, M. Lee, and J. H. Lee, Nonvolatile balanced ternary memory based on the multiferroelectric material $GeSnTe_2$, *J. Phys. Chem. Lett.* 10(23), 7470 (2019)
48. D. Zhao, T. Lenz, G. H. Gelinck, P. Groen, D. Damjanovic, D. M. de Leeuw, and I. Katsouras, Depolarization of multidomain ferroelectric materials, *Nat. Commun.* 10(1), 2547 (2019)
49. S. Baek, H. H. Yoo, J. H. Ju, P. Sriboriboon, P. Singh,

J. Niu, J. H. Park, C. Shin, Y. Kim, and S. Lee, Ferroelectric field-effect-transistor integrated with ferroelectrics heterostructure, *Adv. Sci. (Weinh.)* 9(21), 2200566 (2022)
50. A. I. Khan, A. Keshavarzi, and S. Datta, The future of ferroelectric field-effect transistor technology, *Nat. Electron.* 3(10), 588 (2020)
51. C. Cui, F. Xue, W. J. Hu, and L. J. Li, Two-dimensional materials with piezoelectric and ferroelectric functionalities, *npj 2D Mater. Appl.* 2(1), 18 (2018)
52. M. Dai, Z. Wang, F. Wang, Y. Qiu, J. Zhang, C. Y. Xu, T. Zhai, W. Cao, Y. Fu, D. Jia, Y. Zhou, and P. A. Hu, Two-dimensional van der Waals materials with aligned in-plane polarization and large piezoelectric effect for self-powered piezoelectric sensors, *Nano Lett.* 19(8), 5410 (2019)
53. D. Zhang, H. Wu, C. R. Bowen, and Y. Yang, Recent advances in pyroelectric materials and applications, *Small* 17(51), 2103960 (2021)
54. J. Jiang, L. Zhang, C. Ming, H. Zhou, P. Bose, Y. Guo, Y. Hu, B. Wang, Z. Chen, R. Jia, S. Pendse, Y. Xiang, Y. Xia, Z. Lu, X. Wen, Y. Cai, C. Sun, G. C. Wang, T. M. Lu, D. Gall, Y. Y. Sun, N. Koratkar, E. Fohtung, Y. Shi, and J. Shi, Giant pyroelectricity in nanomembranes, *Nature* 607(7919), 480 (2022)
55. Y. Li, J. Fu, X. Mao, C. Chen, H. Liu, M. Gong, and H. Zeng, Enhanced bulk photovoltaic effect in two-dimensional ferroelectric $CuInP_2S_6$, *Nat. Commun.* 12(1), 5896 (2021)
56. D. Wu, C. Guo, L. Zeng, X. Ren, Z. Shi, L. Wen, Q. Chen, M. Zhang, X. J. Li, C. X. Shan, and J. Jie, Phase-controlled van der Waals growth of wafer-scale 2D $MoTe_2$ layers for integrated high-sensitivity broadband infrared photodetection, *Light Sci. Appl.* 12(1), 5 (2023)
57. K. Tang, Y. Wang, C. Gong, C. Yin, M. Zhang, X. Wang, and J. Xiong, Electronic and photoelectronic memristors based on 2D materials, *Adv. Electron. Mater.* 8(4), 2101099 (2022)
58. H. Duan, S. Cheng, L. Qin, X. Zhang, B. Xie, Y. Zhang, and W. Jie, Low-power memristor based on two-dimensional materials, *J. Phys. Chem. Lett.* 13(31), 7130 (2022)
59. Z. M. Tsikriteas, J. I. Roscow, C. R. Bowen, and H. Khanbareh, Flexible ferroelectric wearable devices for medical applications, *iScience* 24(1), 101987 (2021)
60. X. Mao, J. Fu, C. Chen, Y. Li, H. Liu, M. Gong, and H. Zeng, Nonvolatile electric control of exciton complexes in monolayer $MoSe_2$ with two-dimensional ferroelectric $CuInP_2S_6$, *ACS Appl. Mater. Interfaces* 13(20), 24250 (2021)
61. K. Chang, J. Liu, H. Lin, N. Wang, K. Zhao, A. Zhang, F. Jin, Y. Zhong, X. Hu, W. Duan, Q. Zhang, L. Fu, Q. K. Xue, X. Chen, and S. H. Ji, Discovery of robust in-plane ferroelectricity in atomic-thick SnTe, *Science* 353(6296), 274 (2016)
62. C. C. Chiang, V. Ostwal, P. Wu, C. S. Pang, F. Zhang, Z. Chen, and J. Appenzeller, Memory applications from 2D materials, *Appl. Phys. Rev.* 8(2), 021306 (2021)
63. L. Wang, X. Wang, Y. Zhang, R. Li, T. Ma, K. Leng, Z. Chen, I. Abdelwahab, and K. P. Loh, Exploring ferroelectric switching in α-In_2Se_3 for neuromorphic computing, *Adv. Funct. Mater.* 30(45), 2004609 (2020)
64. Y. Liu, W. Zhou, G. Tang, C. Yang, X. Wang, and J. Hong, Coexistence of magnetism and ferroelectricity in 3D transition-metal-doped SnTe monolayer, *J. Phys. Chem. C* 123(47), 28919 (2019)
65. T. Li, J. Cao, H. Gao, Z. Wang, M. Geiwitz, K. S. Burch, and X. Ling, Epitaxial atomic substitution for MoS_2–MoN heterostructure synthesis, *ACS Appl. Mater. Interfaces* 14(51), 57144 (2022)
66. H. Qiao, C. Wang, W. S. Choi, M. H. Park, and Y. Kim, Ultra-thin ferroelectrics, *Mater. Sci. Eng. Rep.* 145, 100622 (2021)
67. R. K. Vasudevan, N. Balke, P. Maksymovych, S. Jesse, and S. V. Kalinin, Ferroelectric or non-ferroelectric: Why so many materials exhibit "ferroelectricity" on the nanoscale, *Appl. Phys. Rev.* 4(2), 021302 (2017)
68. B. Jiang, J. Iocozzia, L. Zhao, H. Zhang, Y. W. Harn, Y. Chen, and Z. Lin, Barium titanate at the nanoscale: controlled synthesis and dielectric and ferroelectric properties, *Chem. Soc. Rev.* 48(4), 1194 (2019)
69. C. Zhao, Y. Huang, and J. Wu, Multifunctional barium titanate ceramics via chemical modification tuning phase structure, *InfoMat* 2(6), 1163 (2020)
70. T. Mikolajick, M. H. Park, L. Begon-Lours, and S. Slesazeck, From ferroelectric material optimization to neuromorphic devices, *Adv. Mater.* 35(27), 2206042 (2022)
71. M. Wu, 100 years of ferroelectricity, *Nat. Rev. Phys.* 3(11), 726 (2021)
72. H. Sun, J. Gu, Y. Li, T. R. Paudel, D. Liu, J. Wang, Y. Zang, C. Gu, J. Yang, W. Sun, Z. Gu, E. Y. Tsymbal, J. Liu, H. Huang, D. Wu, and Y. Nie, Prominent size effects without a depolarization field observed in ultrathin ferroelectric oxide membranes, *Phys. Rev. Lett.* 130(12), 126801 (2023)
73. X. Jia, R. Guo, B. K. Tay, and X. Yan, Flexible ferroelectric devices: Status and applications, *Adv. Funct. Mater.* 32(45), 2205933 (2022)
74. D. Zhang, P. Schoenherr, P. Sharma, and J. Seidel, Ferroelectric order in van der Waals layered materials, *Nat. Rev. Mater.* 8(1), 25 (2022)
75. Z. L. Yuan, Y. Sun, D. Wang, K. Q. Chen, and L. M. Tang, A review of ultra-thin ferroelectric films, *J. Phys.: Condens. Matter* 33(40), 403003 (2021)
76. J. Y. Li, H. D. Li, X. B. Niu, and Z. M. Wang, Low-dimensional In_2Se_3 compounds: From material preparations to device applications, *ACS Nano* 15(12), 18683 (2021)
77. H. Yang, M. Q. Xiao, Y. Cui, L. F. Pan, K. Zhao, and Z. M. Wei, Nonvolatile memristor based on heterostructure of 2D room-temperature ferroelectric alpha-In_2Se_3 and WSe_2, *Sci. China Inform. Sci.* 62(12), 220404 (2019)
78. S. Zhou, L. You, H. Zhou, Y. Pu, Z. Gui, and J. Wang, Van der Waals layered ferroelectric $CuInP_2S_6$: Physical properties and device applications, *Front. Phys.* 16(1), 13301 (2021)
79. D. Zhang, Z. D. Luo, Y. Yao, P. Schoenherr, C. Sha, Y. Pan, P. Sharma, M. Alexe, and J. Seidel,

Anisotropic ion migration and electronic conduction in van der Waals ferroelectric $CuInP_2S_6$, *Nano Lett.* 21(2), 995 (2021)

80. B. Lin, A. Chaturvedi, J. Di, L. You, C. Lai, R. Duan, J. Zhou, B. Xu, Z. Chen, P. Song, J. Peng, B. Ma, H. Liu, P. Meng, G. Yang, H. Zhang, Z. Liu, and F. Liu, Ferroelectric-field accelerated charge transfer in 2D $CuInP_2S_6$ heterostructure for enhanced photocatalytic H_2 evolution, *Nano Energy* 76, 104972 (2020)
81. A. Jindal, A. Saha, Z. Li, T. Taniguchi, K. Watanabe, J. C. Hone, T. Birol, R. M. Fernandes, C. R. Dean, A. N. Pasupathy, and D. A. Rhodes, Coupled ferroelectricity and superconductivity in bilayer Td–$MoTe_2$, *Nature* 613(7942), 48 (2023)
82. F. Ahmed, A. M. Shafi, D. M. A. Mackenzie, M. A. Qureshi, H. A. Fernandez, H. H. Yoon, M. G. Uddin, M. Kuittinen, Z. Sun, and H. Lipsanen, Multilayer $MoTe_2$ field-effect transistor at high temperatures, *Adv. Mater. Interfaces* 8(22), 2100950 (2021)
83. M. R. Sokolov, K. A. Tumbinskiy, A. I. Zvyagina, I. N. Senchikhin, A. A. Averin, A. E. Aleksandrov, A. R. Tameev, A. A. Ezhov, and M. A. Kalinina, A new 2-methylimidazole-assisted liquid-exfoliation method for a rapid scalable fabrication of chemically pure MoS_2 nanosheets, *Colloid Interface Sci. Commun.* 47, 100604 (2022)
84. S. N. Shirodkar and U. V. Waghmare, Emergence of ferroelectricity at a metal–semiconductor transition in a 1T monolayer of MoS_2, *Phys. Rev. Lett.* 112(15), 157601 (2014)
85. S. Kumar, A. Sharma, Y. T. Ho, A. Pandey, M. Tomar, A. K. Kapoor, E. Y. Chang, and V. Gupta, High performance UV photodetector based on MoS_2 layers grown by pulsed laser deposition technique, *J. Alloys Compd.* 835, 155222 (2020)
86. X. Zhu, D. Li, X. Liang, and W. D. Lu, Ionic modulation and ionic coupling effects in MoS_2 devices for neuromorphic computing, *Nat. Mater.* 18(2), 141 (2019)
87. Y. Sun, G. Niu, W. Ren, X. Meng, J. Zhao, W. Luo, Z. G. Ye, and Y. H. Xie, Hybrid system combining two-dimensional materials and ferroelectrics and its application in photodetection, *ACS Nano* 15(7), 10982 (2021)
88. Y. T. Huang, N. K. Chen, Z. Z. Li, X. P. Wang, H. B. Sun, S. Zhang, and X. B. Li, Two-dimensional In_2Se_3: A rising advanced material for ferroelectric data storage, *InfoMat* 4(8) (2022)
89. C. Chen, H. Liu, Q. Lai, X. Mao, J. Fu, Z. Fu, and H. Zeng, Large-scale domain engineering in two-dimensional ferroelectric $CuInP_2S_6$ via giant flexoelectric effect, *Nano Lett.* 22(8), 3275 (2022)
90. C. Cui, W. J. Hu, X. Yan, C. Addiego, W. Gao, Y. Wang, Z. Wang, L. Li, Y. Cheng, P. Li, X. Zhang, H. N. Alshareef, T. Wu, W. Zhu, X. Pan, and L. J. Li, Intercorrelated in-plane and out-of-plane ferroelectricity in ultrathin two-dimensional layered semiconductor In_2Se_3, *Nano Lett.* 18(2), 1253 (2018)
91. J. Yang, J. Zhou, J. Lu, Z. Luo, J. Yang, and L. Shen, Giant tunnelling electroresistance through 2D sliding ferroelectric materials, *Mater. Horiz.* 9(5), 1422 (2022)
92. L. Li and M. Wu, Binary compound bilayer and multilayer with vertical polarizations: Two-dimensional ferroelectrics, multiferroics, and nanogenerators, *ACS Nano* 11(6), 6382 (2017)
93. M. V. Stern, Y. Waschitz, W. Cao, I. Nevo, K. Watanabe, T. Taniguchi, E. Sela, M. Urbakh, O. Hod, and M. B. Shalom, Interfacial ferroelectricity by van der Waals sliding, *Science* 372(6549), 1462 (2021)
94. X. Hao, H. Wang, and H. Zhang, Engineering application of nanomaterial and ferroelectric domain polarization to the dynamic structure of the surrounding rock of heavy-duty railway with small clear intersection tunnel, *Adv. Mater. Sci. Eng.* 2023, 8354167 (2023)
95. J. Schultheiß, G. Picht, J. Wang, Y. A. Genenko, L. Q. Chen, J. E. Daniels, and J. Koruza, Ferroelectric polycrystals: Structural and microstructural levers for property-engineering via domain-wall dynamics, *Prog. Mater. Sci.* 136, 101101 (2023)
96. C. Weymann, C. Lichtensteiger, S. Fernandez-Peña, A. B. Naden, L. R. Dedon, L. W. Martin, J. M. Triscone, and P. Paruch, Full control of polarization in ferroelectric thin films using growth temperature to modulate defects, *Adv. Electron. Mater.* 6(12), 2000852 (2020)
97. W. Wang, J. Li, H. Liu, and S. Ge, Advancing versatile ferroelectric materials toward biomedical applications, *Adv. Sci. (Weinh.)* 8(1), 2003074 (2021)
98. W. Ding, J. Lu, X. Tang, L. Kou, and L. Liu, Ferroelectric materials and their applications in activation of small molecules, *ACS Omega* 8(7), 6164 (2023)
99. Y. Guo, H. Zhu, and Q. Wang, Piezoelectric effects in surface-engineered two-dimensional group III nitrides, *ACS Appl. Mater. Interfaces* 11(1), 1033 (2019)
100. I. Katsouras, K. Asadi, M. Li, T. B. van Driel, K. S. Kjaer, D. Zhao, T. Lenz, Y. Gu, P. W. Blom, D. Damjanovic, M. Nielsen, and D. M. de Leeuw, The negative piezoelectric effect of the ferroelectric polymer poly(vinylidene fluoride), *Nat. Mater.* 15(1), 78 (2016)
101. M. M. Yang, Z. D. Luo, Z. Mi, J. Zhao, S. P. E, and M. Alexe, Piezoelectric and pyroelectric effects induced by interface polar symmetry, *Nature* 584(7821), 377 (2020)
102. P. Kumbhakar, C. C. Gowda, and C. S. Tiwary, Advance optical properties and emerging applications of 2D materials, *Front. Mater.* 8, 721514 (2021)
103. J. An, X. Zhao, Y. Zhang, M. Liu, J. Yuan, X. Sun, Z. Zhang, B. Wang, S. Li, and D. Li, Perspectives of 2D materials for optoelectronic integration, *Adv. Funct. Mater.* 32(14), 2110119 (2021)
104. Q. Qian, J. Lei, J. Wei, Z. Zhang, G. Tang, K. Zhong, Z. Zheng, and K. J. Chen, 2D materials as semiconducting gate for field-effect transistors with inherent over-voltage protection and boosted ON-current, *npj 2D Mater. Appl.* 3, 24 (2019)
105. T. Afaneh, P. K. Sahoo, I A P. Nobrega, Y. Xin, and H. R. Gutiérrez, Laser-assisted chemical modification of monolayer transition metal dichalcogenides, *Adv. Funct. Mater.* 28(37), 1802949 (2018)
106. V. Shautsova, S. Sinha, L. Hou, Q. Zhang, M. Tweedie, Y. Lu, Y. Sheng, B. F. Porter, H. Bhaskaran, and J. H. Warner, Direct laser patterning and phase transformation of 2D $PdSe_2$ films for on-demand device fabrication, *ACS Nano* 13(12), 14162 (2019)

107. G. G. Naumis, S. Barraza-Lopez, M. Oliva-Leyva, and H. Terrones, Electronic and optical properties of strained graphene and other strained 2D materials: A review, *Rep. Prog. Phys.* 80(9), 096501 (2017)
108. H. Qiu, W. Zhou, and W. Guo, Nanopores in graphene and other 2D materials: A decade's journey toward sequencing, *ACS Nano* 15(12), 18848 (2021)
109. H. Ju, Y. Lee, K. T. Kim, I. H. Choi, C. J. Roh, S. Son, P. Park, J. H. Kim, T. S. Jung, J. H. Kim, K. H. Kim, J. G. Park, and J. S. Lee, Possible persistence of multiferroic order down to bilayer limit of van der Waals material NiI_2, *Nano Lett.* 21(12), 5126 (2021)
110. M. Kruse, U. Petralanda, M. N. Gjerding, K. W. Jacobsen, K. S. Thygesen, and T. Olsen, Two-dimensional ferroelectrics from high throughput computational screening, *npj Comput Mater.* 9(1), 45 (2023)
111. J. Liu and S. T. Pantelides, Pyroelectric response and temperature-induced α-β phase transitions in α-In_2Se_3 and other α-III_2VI_3 (III = Al, Ga, In; VI = S, Se) monolayers, *2D Mater.* 6(2), 025001 (2019)
112. P. Finkel, M. G. Cain, T. Mion, M. Staruch, J. Kolacz, S. Mantri, C. Newkirk, K. Kavetsky, J. Thornton, J. Xia, M. Currie, T. Hase, A. Moser, P. Thompson, C. A. Lucas, A. Fitch, J. M. Cairney, S. D. Moss, A. G. A. Nisbet, J. E. Daniels, and S. E. Lofland, Simultaneous large optical and piezoelectric effects induced by domain reconfiguration related to ferroelectric phase transitions, *Adv. Mater.* 34(7), 2106827 (2022)
113. M. Gabel and Y. Gu, Understanding microscopic operating mechanisms of a van der Waals planar ferroelectric memristor, *Adv. Funct. Mater.* 31(9), 2009999 (2021)
114. K. Liu, T. Zhang, B. Dang, L. Bao, L. Xu, C. Cheng, Z. Yang, R. Huang, and Y. Yang, An optoelectronic synapse based on α-In_2Se_3 with controllable temporal dynamics for multimode and multiscale reservoir computing, *Nat. Electron.* 5(11), 761 (2022)
115. S. Xiao, X. Li, W. Zhang, Y. Xiang, T. Li, X. Niu, J. S. Chen, and Q. Yan, Bilateral interfaces in In_2Se_3–$CoIn_2$–$CoSe_2$ heterostructures for high-rate reversible sodium storage, *ACS Nano* 15(8), 13307 (2021)
116. R. Xue, Z. Shao, X. Yang, Y. Zhang, Z. Fu, Y. Huang, and W. Feng, Self-powered photoelectrochemical photodetectors based on electrochemically exfoliated In_2Se_3 nanosheets, *ACS Appl. Nano Mater.* 5(5), 7036 (2022)
117. R. Moshwan, L. Yang, J. Zou, and Z. G. Chen, Eco-friendly SnTe thermoelectric materials: Progress and future challenges, *Adv. Funct. Mater.* 27(43), 1703278 (2017)
118. K. Chang, J. Liu, H. Lin, N. Wang, K. Zhao, A. Zhang, F. Jin, Y. Zhong, X. Hu, W. Duan, Q. Zhang, L. Fu, Q. K. Xue, X. Chen, and S. H. Ji, Discovery of robust in-plane ferroelectricity in atomic-thick SnTe, *Science* 353(6296), 274 (2016)
119. C. R. Guo, B. C. Qin, D. Y. Wang, and L. D. Zhao, Investigation on halogen-doped n-type SnTe thermoelectrics, *Rare Met.* 41(11), 3803 (2022)
120. F. Xiong, H. B. Tan, C. Xia, and Y. Chen, Strain and doping in two-dimensional SnTe nanosheets: Implications for thermoelectric conversion, *ACS Appl. Nano Mater.* 3(1), 114 (2020)
121. H. Pang, Y. Qiu, D. Wang, Y. Qin, R. Huang, Z. Yang, X. Zhang, and L. D. Zhao, Realizing N-type SnTe thermoelectrics with competitive performance through suppressing Sn vacancies, *J. Am. Chem. Soc.* 143(23), 8538 (2021)
122. J. Chen, C. Zhu, G. Cao, H. Liu, R. Bian, J. Wang, C. Li, J. Chen, Q. Fu, Q. Liu, P. Meng, W. Li, F. Liu, and Z. Liu, Mimicking neuroplasticity via ion migration in van der Waals layered copper indium thiophosphate, *Adv. Mater.* 34(25), 2104676 (2022)
123. X. Jiang, X. Wang, X. Wang, X. Zhang, R. Niu, J. Deng, S. Xu, Y. Lun, Y. Liu, T. Xia, J. Lu, and J. Hong, Manipulation of current rectification in van der Waals ferroionic $CuInP_2S_6$, *Nat. Commun.* 13(1), 574 (2022)
124. D. Wijethunge, L. Zhang, and A. Du, Prediction of two-dimensional ferroelectric metal Mxenes, *J. Mater. Chem. C* 9(34), 11343 (2021)
125. R. Tahir, S. A. Zahra, U. Naeem, D. Akinwande, and S. Rizwan, First observation on emergence of strong room-temperature ferroelectricity and multiferroicity in 2D-$Ti_3C_2T_x$ free-standing MXene film, *RSC Adv.* 12(38), 24571 (2022)
126. R. Tahir, S. Fatima, S. A. Zahra, D. Akinwande, H. Li, S. H. M. Jafri, and S. Rizwan, Multiferroic and ferroelectric phases revealed in 2D $Ti_3C_2T_x$ MXene film for high performance resistive data storage devices, *npj 2D Mater. Appl.* 7(1), 7 (2023)
127. S. Yuan, X. Luo, H. L. Chan, C. Xiao, Y. Dai, M. Xie, and J. Hao, Room-temperature ferroelectricity in $MoTe_2$ down to the atomic monolayer limit, *Nat. Commun.* 10(1), 1775 (2019)
128. A. Weston, E. G. Castanon, V. Enaldiev, F. Ferreira, S. Bhattacharjee, S. Xu, H. Corte-Leon, Z. Wu, N. Clark, A. Summerfield, T. Hashimoto, Y. Gao, W. Wang, M. Hamer, H. Read, L. Fumagalli, A. V. Kretinin, S. J. Haigh, O. Kazakova, A. K. Geim, V. I. Fal'ko, and R. Gorbachev, Interfacial ferroelectricity in marginally twisted 2D semiconductors, *Nat. Nanotechnol.* 17(4), 390 (2022)
129. M. Han, C. Wang, K. Niu, Q. Yang, C. Wang, X. Zhang, J. Dai, Y. Wang, X. Ma, J. Wang, L. Kang, W. Ji, and J. Lin, Continuously tunable ferroelectric domain width down to the single-atomic limit in bismuth tellurite, *Nat. Commun.* 13(1), 5903 (2022)
130. R. Fei, W. Kang, and L. Yang, Ferroelectricity and phase transitions in monolayer group-IV monochalcogenides, *Phys. Rev. Lett.* 117(9), 097601 (2016)
131. K. Chang and S. S. P. Parkin, Experimental formation of monolayer group-IV monochalcogenides, *J. Appl. Phys.* 127(22), 220902 (2020)
132. N. Higashitarumizu, H. Kawamoto, C. J. Lee, B. H. Lin, F. H. Chu, I. Yonemori, T. Nishimura, K. Wakabayashi, W. H. Chang, and K. Nagashio, Purely in-plane ferroelectricity in monolayer SnS at room temperature, *Nat. Commun.* 11(1), 2428 (2020)
133. X. F. Lu, Y. Zhang, N. Wang, S. Luo, K. Peng, L. Wang, H. Chen, W. Gao, X. H. Chen, Y. Bao, G. Liang, and K. P. Loh, Exploring low power and ultrafast memristor on p-type van der Waals SnS, *Nano Lett.*

21(20), 8800 (2021)
134. Y. Luo, N. Mao, D. Ding, M. H. Chiu, X. Ji, K. Watanabe, T. Taniguchi, V. Tung, H. Park, P. Kim, J. Kong, and W. L. Wilson, Electrically switchable anisotropic polariton propagation in a ferroelectric van der Waals semiconductor, *Nat. Nanotechnol.* 18(4), 350 (2023)
135. K. Chang, F. Kuster, B. J. Miller, J. R. Ji, J. L. Zhang, P. Sessi, S. Barraza-Lopez, and S. S. P. Parkin, Microscopic manipulation of ferroelectric domains in SnSe monolayers at room temperature, *Nano Lett.* 20(9), 6590 (2020)
136. H. Li, Q. Zhang, C. C. R. Yap, B. K. Tay, T. H. T. Edwin, A. Olivier, and D. Baillargeat, From bulk to monolayer MoS_2: Evolution of Raman scattering, *Adv. Funct. Mater.* 22(7), 1385 (2012)
137. E. Gao, S. Z. Lin, Z. Qin, M. J. Buehler, X. Q. Feng, and Z. Xu, Mechanical exfoliation of two-dimensional materials, *J. Mech. Phys. Solids* 115, 248 (2018)
138. K. S. Novoselov, S. V. Morozov, D. Jiang, Y. Zhang, S. V. Dubonos, I. V. Grigorieva, and A. A. Firsov, Electric field effect in atomically thin carbon films, *Science* 306(5696), 666 (2004)
139. J. N. Coleman, M. Lotya, A. O'Neill, S. D. Bergin, P. J. King, et al., Liquid exfoliation of layered materials, *Science* 331(6017), 568 (2013)
140. C. Chang, W. Chen, Y. Chen, Y. Chen, Y. Chen, et al., Recent progress on two-dimensional materials, *Acta Phys.-Chim. Sin.* 37(12), 2108017 (2021)
141. Z. Lin, Y. Liu, U. Halim, M. Ding, Y. Liu, Y. Wang, C. Jia, P. Chen, X. Duan, C. Wang, F. Song, M. Li, C. Wan, Y. Huang, and X. Duan, Solution-processable 2D semiconductors for high-performance large-area electronics, *Nature* 562(7726), 254 (2018)
142. J. N. Coleman, M. Lotya, A. O'Neill, S. D. Bergin, P. J. King, et al., Two-dimensional nanosheets produced by liquid exfoliation of layered materials, *Science* 331(6017), 568 (2011)
143. X. Cai, Y. Luo, B. Liu, and H. M. Cheng, Preparation of 2D material dispersions and their applications, *Chem. Soc. Rev.* 47(16), 6224 (2018)
144. M. Chhowalla, H. S. Shin, G. Eda, L. J. Li, K. P. Loh, and H. Zhang, The chemistry of two-dimensional layered transition metal dichalcogenide nanosheets, *Nat. Chem.* 5(4), 263 (2013)
145. J. D. Yao, Z. Q. Zheng, and G. W. Yang, Production of large-area 2D materials for high-performance photodetectors by pulsed-laser deposition, *Prog. Mater. Sci.* 106, 100573 (2019)
146. N. A. Shepelin, Z. P. Tehrani, N. Ohannessian, C. W. Schneider, D. Pergolesi, and T. Lippert, A practical guide to pulsed laser deposition, *Chem. Soc. Rev.* 52(7), 2294 (2023)
147. R. Rashid, F. C. C. Ling, S. P. Wang, K. Xiao, X. Cui, Q. Rao, and D. K. Ki, IP and OOP ferroelectricity in hexagonal γ-In_2Se_3 nanoflakes grown by chemical vapor deposition, *J. Alloys Compd.* 870, 159344 (2021)
148. J. Zhou, Q. Zeng, D. Lv, L. Sun, L. Niu, W. Fu, F. Liu, Z. Shen, C. Jin, and Z. Liu, Controlled synthesis of high-quality monolayered α-In_2Se_3 via physical vapor deposition, *Nano Lett.* 15(10), 6400 (2015)
149. Y. Huang, Y. H. Pan, R. Yang, L. H. Bao, L. Meng, et al., Universal mechanical exfoliation of large-area 2D crystals, *Nat. Commun.* 11(1), 2453 (2020)
150. J. Gao, Y. Zheng, W. Yu, Y. Wang, T. Jin, X. Pan, K. P. Loh, and W. Chen, Intrinsic polarization coupling in 2D α-In_2Se_3 toward artificial synapse with multimode operations, *SmartMat* 2(1), 88 (2021)
151. Z. Wang and W. Zhu, Tunable band alignments in 2D ferroelectric α-In_2Se_3 based van der Waals heterostructures, *ACS Appl. Electron. Mater.* 3(11), 5114 (2021)
152. B. Lv, W. Xue, Z. Yan, R. Yang, H. Wu, P. Wang, Y. Zhang, J. Hou, W. Zhu, and X. Xu, Control of photocurrent and multi-state memory by polar order engineering in 2H-stacked α-In_2Se_3 ferroelectric, *Sci. China Mater.* 65(6), 1639 (2022)
153. Y. Zhang, L. Wang, H. Chen, T. Ma, X. Lu, and K. P. Loh, Analog and digital mode α-In_2Se_3 memristive devices for neuromorphic and memory applications, *Adv. Electron. Mater.* 7(12), 2100609 (2021)
154. S. Wan, Q. Peng, Z. Wu, and Y. Zhou, Nonvolatile ferroelectric memory with lateral β/α/β In_2Se_3 heterojunctions, *ACS Appl. Mater. Interfaces* 14(22), 25693 (2022)
155. Y. Liu, Y. Wu, B. Wang, H. Chen, D. Yi, and K. Liu, Versatile memristor implemented in van der Waals $CuInP_2S_6$, *Nano Res.* 16(6), (2023)
156. B. Li, S. Li, H. Wang, L. Chen, L. Liu, X. Feng, Y. Li, J. Chen, X. Gong, and K. W. Ang, An electronic synapse based on 2D ferroelectric $CuInP_2S_6$, *Adv. Electron. Mater.* 6(12), 2000760 (2020)
157. P. Li, A. Chaturvedi, H. Zhou, G. Zhang, Q. Li, J. Xue, Z. Zhou, S. Wang, K. Zhou, Y. Weng, F. Zheng, Z. Shi, E. H. T. Teo, L. Fang, and L. You, Electrostatic coupling in $MoS_2/CuInP_2S_6$ ferroelectric vdW heterostructures, *Adv. Funct. Mater.* 32(29), 2201359 (2022)
158. S. R. Jian, J. Y. Juang, C. W. Luo, S. A. Ku, and K. H. Wu, Nanomechanical properties of GaSe thin films deposited on Si(111) substrates by pulsed laser deposition, *J. Alloys Compd.* 542, 124 (2012)
159. K. C. Kwon, Y. Zhang, L. Wang, W. Yu, X. Wang, I. H. Park, H. S. Choi, T. Ma, Z. Zhu, B. Tian, C. Su, and K. P. Loh, In-plane ferroelectric tin monosulfide and its application in a ferroelectric analog synaptic device, *ACS Nano* 14(6), 7628 (2020)
160. P. C. Shen, Y. Lin, H. Wang, J. H. Park, W. S. Leong, A. Y. Lu, T. Palacios, and J. Kong, CVD technology for 2-D materials, *IEEE Trans. Electron Dev.* 65(10), 4040 (2018)
161. D. Vernardou, Special issue: Advances in chemical vapor deposition, *Materials (Basel)* 13(18), 4167 (2020)
162. W. F. Io, S. Yuan, S. Y. Pang, L. W. Wong, J. Zhao, and J. Hao, Temperature- and thickness-dependence of robust out-of-plane ferroelectricity in CVD grown ultrathin van der Waals α-In_2Se_3 layers, *Nano Res.* 13(7), 1897 (2020)
163. C. Muratore, A. A. Voevodin, and N. R. Glavin, Physical vapor deposition of 2D van der Waals materials: A review, *Thin Solid Films* 688, 137500 (2019)
164. B. Liu, Q. Han, L. Li, S. Zheng, Y. Shu, J. A. Pedersen, and Z. Wang, Synergistic effect of metal cations

and visible light on 2D MoS_2 nanosheet aggregation, *Environ. Sci. Technol.* 55(24), 16379 (2021)

165. P. D. Taylor, S. A. Tawfik, and M. J. S. Spencer, Ferroelectric van der Waals heterostructures of $CuInP_2S_6$ for non-volatile memory device applications, *Nanotechnology* 34(6), 065701 (2023)
166. W. Yang, B. Cheng, J. Hou, J. Deng, X. Ding, J. Sun, and J. Z. Liu, Writing-speed dependent thresholds of ferroelectric domain switching in monolayer α-In_2Se_3, *Small Methods* 7(6), 2300050 (2023)
167. Y. Yan, M. Xiang, X. Wang, T. Xu, and F. Xuan, Ferroelectric domain wall in two-dimensional GeS, *J. Appl. Phys.* 132(7), 074302 (2022)
168. F. Xue, X. He, Y. Ma, D. Zheng, C. Zhang, L. J. Li, J. H. He, B. Yu, and X. Zhang, Unraveling the origin of ferroelectric resistance switching through the interfacial engineering of layered ferroelectric-metal junctions, *Nat. Commun.* 12(1), 7291 (2021)
169. S. Zhou, L. Liao, J. Chen, Y. Yu, Z. Lv, M. Yang, B. Yao, S. Zhang, G. Peng, Z. Huang, Y. Liu, X. Qi, and G. Wang, Periodic ferroelectric stripe domains in α-In_2Se_3 nanoflakes grown via reverse-flow chemical vapor deposition, *ACS Appl. Mater. Interfaces* 15(19), 23613 (2023)
170. Y. Zhai, P. Xie, J. Hu, X. Chen, Z. Feng, Z. Lv, G. Ding, K. Zhou, Y. Zhou, and S. T. Han, Reconfigurable 2D-ferroelectric platform for neuromorphic computing, *Phys. Rev. Appl.* 10(1), 011408 (2023)
171. W. Li, Y. Guo, Z. Luo, S. Wu, B. Han, W. Hu, L. You, K. Watanabe, T. Taniguchi, T. Alava, J. Chen, P. Gao, X. Li, Z. Wei, L. W. Wang, Y. Y. Liu, C. Zhao, X. Zhan, Z. V. Han, and H. Wang, A gate programmable van der Waals metal-ferroelectric-semiconductor vertical heterojunction memory, *Adv. Mater.* 35(5), 2208266 (2023)
172. Y. Wang, W. Li, Y. Guo, X. Huang, Z. Luo, S. Wu, H. Wang, J. Chen, X. Li, X. Zhan, and H. Wang, A gate-tunable artificial synapse based on vertically assembled van der Waals ferroelectric heterojunction, *J. Mater. Sci. Technol.* 128, 239 (2022)
173. A. Abnavi, R. Ahmadi, A. Hasani, M. Fawzy, M. R. Mohammadzadeh, T. De Silva, N. Yu, and M. M. Adachi, Free-standing multilayer molybdenum disulfide memristor for brain-inspired neuromorphic applications, *ACS Appl. Mater. Interfaces* 13(38), 45843 (2021)
174. K. Wang, J. Chen, and X. Yan, MXene Ti_3C_2 memristor for neuromorphic behavior and decimal arithmetic operation applications, *Nano Energy* 79, 105453 (2021)
175. Y. Yoon, K. Ganapathi, and S. Salahuddin, How good can monolayer MoS_2 transistors be, *Nano Lett.* 11(9), 3768 (2011)
176. A. B. Loginov, P. V. Fedotov, S. N. Bokova-Sirosh, I. V. Sapkov, D. N. Chmelenin, R. R. Ismagilov, E. D. Obraztsova, B. A. Loginov, and A. N. Obraztsov, Synthesis, structural, and photoluminescence properties of MoS_2 nanowall films, *Phys. Status Solidi B* 260(6), 2200481 (2022)
177. T. Shimada, K. Minaguro, T. Xu, J. Wang, and T. Kitamura, *Ab initio* study of ferroelectric critical size of SnTe low-dimensional nanostructures, *Nanomaterials (Basel)* 10(4), 732 (2020)